TOXICOLOGICAL SCIENCES **139(2)**, 432–451 2014
doi: 10.1093/toxsci/kfu048
Advance Access publication March 10, 2014

Regulation of Copper Transport Crossing Brain Barrier Systems by Cu-ATPases: Effect of Manganese Exposure

Xue Fu, Yanshu Zhang, Wendy Jiang, Andrew Donald Monnot, Christopher Alexander Bates, and Wei Zheng[1]

School of Health Sciences, Purdue University, West Lafayette, Indiana 47907

[1]To whom correspondence should be addressed at School of Health Science, Purdue University, 550 Stadium Mall Drive, CIVL 1173, West Lafayette, IN 47907. Fax: (765) 496-1377. E-mail: wzheng@purdue.edu.

Received January 8, 2014; accepted March 3, 2014

Regulation of cellular copper (Cu) homeostasis involves Cu-transporting ATPases (Cu-ATPases), i.e., ATP7A and ATP7B. The question as to how these Cu-ATPases in brain barrier systems transport Cu, i.e., toward brain parenchyma, cerebrospinal fluid (CSF), or blood, remained unanswered. This study was designed to characterize roles of Cu-ATPases in regulating Cu transport at the blood-brain barrier (BBB) and blood-CSF barrier (BCB) and to investigate how exposure to toxic manganese (Mn) altered the function of Cu-ATPases, thereby contributing to the etiology of Mn-induced parkinsonian disorder. Studies by quantitative real-time RT-PCR (qPCR), Western blot, and immunocytochemistry revealed that both Cu-ATPases expressed abundantly in BBB and BCB. Transport kinetic studies by *in situ* brain infusion and ventriculo-cisternal (VC) perfusion in Sprague Dawley rat suggested that the BBB was a major site for Cu entry into brain, whereas the BCB was a predominant route for Cu efflux from the CSF to blood. Confocal evidence showed that the presence of excess Cu or Mn in the choroid plexus cells led to ATP7A relocating toward the apical microvilli facing the CSF, but ATP7B toward the basolateral membrane facing blood. Mn exposure inhibited the production of both Cu-ATPases. Collectively, these data suggest that Cu is transported by the BBB from the blood to brain, which is mediated by ATP7A in brain capillary. By diffusion, Cu ions move from the interstitial fluid into the CSF, where they are taken up by the BCB. Within the choroidal epithelial cells, Cu ions are transported by ATP7B back to the blood. Mn exposure alters these processes, leading to Cu dyshomeostasis-associated neuronal injury.

Key words: **copper; Cu-ATPases; copper transport; blood-brain barrier; blood-CSF barrier; manganese.**

ABBREVIATIONS

BBB	blood-brain barrier
BCB	blood-cerebrospinal fluid barrier
CSF	cerebrospinal fluid
Cu	copper
Mn	manganese

Copper (Cu) serves as a required cofactor for a number of enzymes such as tyrosinase, cytochrome c oxidase, superoxide dismutase, and ceruloplasmin in diverse biochemical reaction in the body. The excessive cellular amount of Cu ions, however, can readily interact with oxygen, resulting in the generation of hydroxyl radicals. Cu dyshomeostasis in the brain has been linked to several neurodegenerative disorders, such as idiopathic Parkinson's disease (IPD), Alzheimer's disease (AD), prion disease, and amyotrophic lateral sclerosis (ALS) (Gaggelli *et al.*, 2006; Kiaei *et al.*, 2004; Sparks and Schreurs, 2003; Strausak *et al.*, 2001). Human case-control studies have found a significant high level of Cu in the cerebrospinal fluid (CSF) of patients with IPD, AD, and ALS than control subjects (Bocca *et al.*, 2006; Gorell *et al.*, 1999; Hozumi *et al.*, 2011; Squitti *et al.*, 2009; Strozyk *et al.*, 2009). Brain Cu homeostasis is suggested to be regulated by brain barrier systems, i.e., the blood-brain barrier (BBB) and blood-CSF barrier (BCB) (Zheng and Monnot, 2012); however, the precise mechanism remains unknown.

Available data in literature indicate that at the cell surface, the Cu uptake is mediated by Cu transporter 1 (CTR1) and divalent metal transporter 1 (DMT1). Upon entering the cell, Cu is carried by a Cu chaperone ATOX-1 and delivered to the Cu-transporting ATPases (Cu-ATPases), i.e., ATP7A and ATP7B, which are located in the trans-Golgi network (TGN) and perform a dual role in either transporting Cu into the Golgi lumen for the incorporation of cuproenzymes under the basal Cu level, or expelling Cu to extracellular space by loading excess Cu ions into vesicles for the exocytosis when the intracellular Cu level exceeds the need (Arredondo *et al.*, 2003; Petris *et al.*, 1996; Zhou and Gitschier, 1997). Genetic defects in ATP7A and ATP7B can cause Cu deficiency and overload in the liver and brain, leading to clinically well-defined Menkes and Wilson's diseases, representatively. Both Cu-ATPases, ATP7A and ATP7B, have been shown to express highly in the brain capillary endothelia (Qian *et al.*, 1998) and choroidal epithelia (Choi and Zheng, 2009; Iwase *et al.*, 1996; Kuo *et al.*, 1997). Although ATP7A and ATP7B share ~60% amino acid identity, they have different trafficking patterns in polarized cells. ATP7A facili-

tates Cu transport from the TGN to the basolateral surface facing the blood stream in intestinal enterocytes (Nyasae *et al.*, 2007), whereas ATP7B redistributes toward the apical membrane facing the biliary duct in hepatocytes (Malhi *et al.*, 2002). However, how ATP7A and ATP7B mediate Cu transport in brain capillary endothelial and choroidal epithelial cells remained elusive.

Manganese (Mn), an essential trace element for human health, can be toxic upon occupational or dietary overexposure. Mn neurotoxicity, namely manganism, exhibits signs and syndromes that similar, but identical, to IPD (Barbeau *et al.*, 1976; Crossgrove and Zheng, 2004; Gaggelli *et al.*, 2006; Jiang *et al.*, 2006, 2007; Racette *et al.*, 2012). High Cu concentrations have been reported in blood of Mn-exposed workers and parkinsonian patients (Jiang *et al.*, 2007, Squitti *et al.*, 2009; Wang *et al.*, 2008a), as well as in brains of Mn-exposed primates or rodents (Guilarte and Chen, 2007; Lai *et al.*, 1999; Zheng *et al.*, 2009). Our most recent animal study using a murine subchronic Mn exposure model shows a significant elevation of Cu concentrations in striatum, hippocampus, motor cortex and choroid plexus (Zheng *et al.*, 2009). Upon exposure, Mn has been shown to accumulate in the global pallidus by magnetic resonance imaging (MRI) (Guilarte *et al.,* 2006; Jiang *et al.*, 2007; Uchino *et al.,* 2007). The information on whether Mn accumulated in the BBB was not available, yet Mn exposure is known to result in a significant increase of Mn levels in the BCB (Zheng *et al.*, 2009). These observations prompted us to question if Mn exposure disrupted Cu regulation at brain barriers, leading to the dyshomeostasis of Cu in brain which may become a causal factor that contributes to the etiology of manganism.

Purposes of the current study were (1) to characterize the roles of ATP7A and ATP7B in regulating Cu transport at the BBB and BCB by examining their intracellular trafficking in specified brain barrier cells and their responses to increased cellular Cu status; and (2) to investigate how Mn exposure, in *in-vivo* animal or *in-vitro* cell culture models, affected the expression and function of ATP7A and ATP7B. Understanding the Cu regulatory mechanism at brain barrier systems will shed light on the etiology of several Cu-associated neurodegenerative diseases, including Mn-induced parkinsonian disorder.

MATERIALS AND METHODS

Chemicals. Chemical reagents were purchased from the following sources: Mn chloride tetrahydrate ($MnCl_2{\cdot}4H_2O$) from Fisher Scientific (Pittsburgh, PA); Cu chloride ($CuCl_2$), calcium chloride ($CaCl_2$), hydroxyethyl piperazineethanesulfonic acid (HEPES), monoclonal antimouse β-actin antibody, 2-mercaptoethanol, phenylmethylsulfonyl fluoride (PMSF), polyacrylamide and tetramethyl-ethylenediamine (TEMED), epidermal growth factor (EGF), basic fibroblast growth factor (bFGF), and 0.25% trypsin-EDTA from Sigma Chemicals (St Louis, MO); Fluor Alexa-488 conjugated secondary antibody, TRIzol reagent, collagen I (rat tail), fetal bovine serum (FBS), gentamicin, penicillin and streptomycin, alpha-type minimum essential medium (α-MEM), Hank's Balanced Salted Solution (HBSS), silencer select predesigned ATP7A, ATP7B and negative control no. 1 siRNA, and lipofectamine RNAiMAX from Life Technologies (Carlsbad, CA); protease inhibitor cocktail-Calbiochem (San Diego, CA); Ham's F10, Dulbecco's Modified Eagle's Medium (DMEM), and geneticin from Cellgro (Manassas, VA); rabbit polyclonal anti-ATP7A and ATP7B antibodies from Santa Cruz Biotechnology (Santa Cruz, CA); Tris base, glycine, sodium dodecyl sulfate (SDS), 2× Laemmli sample buffer, Triton X-100, cDNA synthesis kit, iTaq Universal SYBR Green Supermix, and clarity Western ECL substrate from Bio-Rad (Hercules, CA); pronase and protease from Calbiochem (La Jolla, CA), and collagen-coated and regular Transwell-COL inserts from Corning (Cambridge, MA). The rabbit polyclonal ATP7B antibody (Cat. no. sc-33826) is raised against amino acids 1372–1465 mapping within a C-terminal cytoplasmic domain of ATP7B of human origin. All reagents were of analytical grade, HPLC grade, or the best available pharmaceutical grade.

Radioactive $^{64}CuCl_2$ (specific activity 15-30 mCi/μg) was purchased from the Mallinckrodt Institute of Radiology, Washington University (St Louis, MO). ^{14}C-sucrose (specific activity: 495 mCi/mmol) was purchased from Moravek Biochemicals, Inc. (Brea, CA), and Eco-lite-(+) scintillation cocktail from MP Biomedicals (Irvine, CA).

Experimental design. Part 1 studies were designed to determine the cellular expression and trafficking of ATP7A and ATP7B in the BBB and to investigate whether Mn exposure altered the Cu transport across the BBB by acting on both Cu-ATPases. An *in situ* brain perfusion technique was used to determine the Cu-uptake kinetics in the BBB. The RBE4 cells were used as an *in vitro* model to study Cu-ATPases function in the BBB.

Part 2 studies were designed to study the cellular expression and trafficking of ATP7A and ATP7B in the BCB and to explore the effect of Mn exposure on the expression and function of both enzymes in the BCB. An *in situ* ventriculo-cisternal (VC) perfusion technique was used to determine the Cu clearance by the BCB. The choroidal Z310 cells and primary choroidal epithelial cells were cultured for experiments as an *in vitro* model of BCB.

In both BBB and BCB studies, the atomic absorption spectroscopy (AAS), immunohistochemistry, quantitative real-time RT-PCR (qPCR), and Western blot were used to determine the metal concentrations, subcellular trafficking, and expression levels of ATP7A and ATP7B in barrier cells.

Animals and Mn administration. Male Sprague Dawley rats were purchased from the Harlan Laboratories (Indianapolis, IN). At the time of use, rats were 10 weeks old weighing 220–250 g. Upon arrival, animals were housed in a temperature-

controlled, 12-h light/dark cycle room and allowed to acclimate for 1 week prior to experimentation. Animals had free access to tap water and pellet Purina semi-purified rat chow (Purina Mills Test Diet, 5755C; Purina Mills, Richmond, Inc.). The study was conducted in compliance with the regulation and approved by the Animal Care and Use Committee of Purdue University.

$MnCl_2 \cdot 4H_2O$ dissolved in sterile saline was administrated to rats by ip injection of 6 mg Mn/kg, once per day, 5 days per week, for four consecutive weeks; the dose regiment was chosen based on earlier Mn neurotoxicity studies done in this laboratory (Zheng *et al.*, 1998, 2000). The daily equivalent volume of sterile saline was given to control animals. Twenty-four hours after the last injection, rats were anesthetized with ketamine/xylazine (75:10 mg/kg, 1 mg/kg, ip) for *in situ* brain perfusion in Part 1 studies or *in situ* VC perfusion in Part 2 studies. CSF samples, free of blood, were collected using 26G butterfly needle by inserting the needle between the protuberance and the spine of the atlas, and blood samples were obtained from the vena cava for serum preparation. Rat brains were dissected to harvest the choroid plexus in lateral and third ventricles, hippocampus (HP), striatum (ST), and frontal cortex (FC). Samples were freshly analyzed or stored at −80°C for later analysis.

Determination of Mn and Cu concentrations by AAS. All brain samples were digested with concentrated ultrapure nitric acid in a MARSXpress microwave-accelerated reaction system. Serum and CSF samples were digested overnight with nitric acid in the oven at 55°C. An Agilent Technologies 200 Series SpectrAA with a GTA 120 graphite tube atomizer was used to quantify Mn and Cu concentrations. Digested samples were diluted by 50, 500, or 1000 times with 1.0% (vol/vol) HNO_3 in order to keep the reading within the concentration range of standard curves. Ranges of calibration standards for Mn and Cu were 0–5 and 0–25 μg/l, respectively. Detection limits for Mn and Cu were 0.09 and 0.9 ng/ml, respectively, of the assay solution. Intraday precision of the method for Mn and Cu were 2.9 and 1.6%, respectively, and the interday precision were 3.3 and 3.7%, respectively (Zheng *et al.*, 1998, 1999, 2009).

In situ *brain perfusion study.* *In situ* brain infusion technique can accurately deliver a known amount of testing drug/toxicant to brain. Based on the amount of metal in brain parenchyma, which is free of cerebral capillaries, in relevance to a given amount of metal in perfusate within a given time frame, the unidirectional influx of metal can be obtained. The method has been well established in the PI's laboratory and routinely used in our research. A detailed description can be found in a technical chapter written by Zheng and Segal (2005). Briefly, the rat was anesthetized with ketamine/xylazine (75:10 mg/kg, 1 mg/kg, ip); the right common carotid artery was exposed and a small cut on the artery was made. After insertion of a polyethylene catheter (PE-10) tubing (toward the brain), ligations of the pterygopalatine, occipital, superior thyroid, and external carotid arteries were made to ensure the perfusate entering exclusively to the internal carotid artery. The brain was perfused with a Ringer solution (containing in g/l: NaCl 7.31, KCl 0.356, $NaHCO_3$ 2.1, KH_2PO_4 0.166, $MgSO_4 \cdot 3H_2O$ 0.213, glucose 1.50, and sodium pyruvate 1 mmol/l and $CaCl_2$ 2.5 mmol/l) at a flow rate of 9 ml/min by a Mini-Pump (VWR). Prior to the start of the experiment, the solution was adjusted to pH 7.4, filtered and pregassed with 5% CO_2-95% O_2. The "hot" solution, which contained radioisotopes of 0.5 μCi/ml of ^{14}C-sucrose (as a space marker) and 30 μCi/ml of ^{64}Cu, and 2μM $CuCl_2$ in pregassed Ringer solution, was delivered by a separate "hot" syringe pump (Harvard Compact Infusion Pump, Model 11 Plus) to the cannulated internal carotid artery at the flow rate of 1 ml/min. Thus, the total flow rate of perfusion was 10 ml/min. To prevent recirculation of the rat blood, the left ventricle of the heart was cut before the start of perfusion.

At the end of the 2-min "hot" perfusion, the "hot" pump was switched off and the Mini-pump stayed on for another 1 min for washing. During the washing time, CSF sample was collected from the cisterna magna. Blood was collected from the inferior vena cava. The brain was removed from the skull and placed on a filter paper, saturated with saline. One half of the brain was used for capillary separation and the other half for regional brain uptake studies. Choroid plexus from three rats (in the same treatment group) were pooled as $n = 1$ (due to the small tissue mass). Five such tissue pools (15 rats in total) from the same group were used for statistical analyses ($n = 5$). HP, ST, and FC were dissected; the capillary was separated from brain parenchyma by the "capillary depletion" method described below.

Separation of capillary from brain parenchyma. The capillary depletion method allows to separate brain capillary fraction from brain parenchyma so that Cu retained in the capillary can be distinguished from Cu presented in the brain parenchyma tissue (without blood vessels). The capillary separation was carried out as previously described (Choi and Zheng, 2009; Deane *et al.*, 2004; Preston *et al.*, 1995). Briefly, the ice chilled brain tissue was weighed and homogenized in a 3-volume ice-cold homogenization buffer (HB-1) solution (g/ml, wt/vol) with eight strokes in a 1-ml dounce tissue grinder (Wheaton, Millville, NJ). The HB-1 solution contained (mmol/l): HEPES 10, NaCl 141, KCl 4, $MgSO_4$ 1.0, NaH_2PO_4 1.0, $CaCl_2$ 2.5, and glucose 10, at pH 7.4. A 4-volume 30% Dextran-70 to the brain weight (vol/wt) was then added to the brain-buffer mix in a ratio of 1:3:4 (brain:buffer:dextran) for three additional strokes. The homogenate was spun at 5400 × g for 15 min at 4°C. The supernatant (capillary-depleted parenchyma) and pellet (capillary-enriched fraction) were separated carefully. The presence of networks of brain vessels in the pellet and a vasculature-depleted supernatant were confirmed by the light microscopy. The radioactivities in the supernatant and pellet of brain tissues and in choroid plexus were counted. Freshly separated capillary without *in situ* brain perfusion was also prepared in the same man-

ner and analyzed for mRNA and proteins levels of ATP7A and ATP7B.

Uptake kinetics calculation. ^{64}Cu uptake was expressed as a volume of distribution, V_d, and calculated by formula (1):

$$V_d\,(\mathrm{ml/g}) = \frac{C_{\mathrm{tissue}} \text{ or } C_{\mathrm{CSF}}}{C_{\mathrm{perfusate}}} \quad (1)$$

where C_{tissue} or C_{CSF} are DPM/g of brain tissue or CSF, and $C_{\mathrm{perfusate}}$ are DPM/ml of the perfusion fluid. V_d for the capillaries was calculated from DPM/g. The unidirectional uptake rates, K_{in} (μl/s/g), corresponding to the slope of the uptake curve was calculated using the linear regression analysis of V_d against the perfusion time (T, s) by the formula (2),

$$V_d = K_{\mathrm{in}}T + V_i \quad (2)$$

where V_i is the ordinate intercept of the regression line. ^{64}Cu uptake rate (K_{in}) was corrected for the residual radioactivity by deducting V_d for ^{14}C-sucrose from the total ^{64}Cu distributing volume. The study allowed us to obtain Cu transport constants (K_{in}) to the choroid plexus, CSF, selected brain regional parenchyma, and capillary.

In situ *VC perfusion study.* The VC perfusion technique has been well established and routinely used in this laboratory (Deane *et al.*, 2004; Monnot *et al.*, 2011; Wang *et al.*, 2008b). In brief, at the end of the treatment, rats were anesthetized and immobilized in a stereotaxic device. A midline cutaneous incision was made from forehead to neck to expose the surface of the skull. A hole for the insertion of guide cannula was made in the skull by a small drill bit (Plastics One Inc., Roanoke, VA). The cannula was implanted into the lateral ventricle according to the following parameters on three scales: 0.8 mm posterior to bregma, 1.4 mm lateral to midline, and 4.0 mm vertical inserted into the guide cannula for lateral ventricle perfusion, which was controlled by a pump-driven syringe filled with the artificial CSF (a-CSF). The pregassed a-CSF contained 35 μCi/ml of ^{64}Cu with the final concentration of 5μM $CuCl_2$ and 0.5 μCi/ml of ^{14}C-sucrose, was delivered to the lateral ventricle at a rate of 28 μl/min controlled by a micropump (Harvard Syringe Pump, Model 11 Plus). A 26G butterfly needle was inserted with an appropriate angle into the cistern magna to collect the CSF outflow by 10-min intervals throughout the 90-min perfusion. The CSF volume was determined by its weight assuming CSF density of 1 g/ml. Additional anesthesia was given to the rat in the hindquarter muscle as needed. Animal's body temperature was maintained at 37°C using a heating pad during the perfusion. At the end of the perfusion, the animal was decapitated, the brain was removed, and choroid plexus tissues were harvested from lateral and third ventricles. Samples were counted to obtain ^{64}Cu and ^{14}C radioactivities.

Cell culture and treatments. The rat brain endothelial (RBE4) cells were used for BBB studies (Lagrange *et al.*, 1999). The characteristics, culture, and maintenance procedures of this cell line were described in previous publications (Régina *et al.*, 1999; Yang and Aschner 2003). Briefly, RBE4 cells were grown in collagen-coated Petri dishes in a culture medium containing 50% α-MEM and 50% Ham's F10 (vol/vol) supplemented with 10% FBS, 2mM glutamine, 100 U/ml penicillin, 100 μg/ml streptomycin, and 300 μg/ml geneticin (G418). The cultures were maintained in a humidified 37°C incubator with 95% air-5% CO_2.

The choroidal epithelial Z310 cell line was originally developed from the murine choroid plexus by this laboratory. The characteristics, culture, and maintenance procedures of this cell line were described in the previous publications (Li *et al.*, 2005; Wang *et al.*, 2006; Zheng and Zhao, 2002). Briefly, Z310 cells were grown in DMEM medium supplemented with 10% FBS, 100 U/ml penicillin, 100 μg/ml streptomycin, 50 μg/ml gentamicin sulfate, and 10 ng/ml EGF, in a humidified incubator with 95% air-5% CO_2 at 37°C, and were passaged twice a week.

Autoclaved $MnCl_2$ (25mM) stocking solution was prepared by dissolving $MnCl_2{\cdot}4H_2O$ in sterile saline. The cells were treated with the working concentration of 100μM $MnCl_2$ for 12, 24, or 48 h in this study. The concentration was selected based on previous *in vivo* Mn studies by this and other laboratories (Li *et al.*, 2005; Parenti *et al.*, 1988; Reaney and Smith, 2005; Vescovi *et al.*, 1991; Wang *et al.*, 2006; Zheng *et al.*, 1999).

Subcellular Cu-ATPases distribution in choroid plexus tissues. To study the subcellular distribution of ATP7A and ATP7B in the choroid plexus tissue as affected by Cu, choroid plexus tissues from lateral and third ventricles were freshly dissected from control rats and immediately incubated in the a-CSF containing 0, 5, or 50μM $CuCl_2$, at 37°C, for 1 h. At the end of the incubation, plexus tissues were fixed in 4% paraformaldehyde for immunofluorescent staining and confocal microscopic studies.

Immunofluorescent staining and confocal microscopy. Glass coverslips were sterilized with 75% ethanol and coated with collagen for RBE4 culture in six-well plate. RBE4 or Z310 cells were seeded at a density of 3×10^5/well, allowed to grow for 24 h to achieve 50% confluence, and then treated with 100μM $MnCl_2$ for 24 h. At the end of treatment, cells were stained with mito-tracker, fixed in 4% paraformaldehyde and permeabilized in 0.1% Triton X-100 at room temperature, followed by three washes with phosphate-buffered saline (PBS) between each two steps. After blocking with 1% bovine serum albumin (BSA) for 1 h at room temperature, cells were incubated with antirabbit polyclonal ATP7A or ATP7B primary antibodies (1:1000) in 1% BSA at 4°C, overnight, followed by incubation with Fluor Alexa-488 conjugated secondary antibody (1:1000) at room temperature for 1 h. Glass coverslips were mounted to objective slides for confocal microscopy observation. The negative

control was established by using only the secondary antibody to reflect nonspecific staining on the background. Slides were prepared using Gold Anti-Fade (Invitrogen, Carlsbad, CA) to avoid fluorescent bleaching for confocal microscopic examination.

To acquire images, slides were mounted on the stage of a Nikon inverted confocal laser-scanning microscope and viewed through a ×60 oil-immersion objective (Plan Apo, ×60/1.40 oil, W.D. 0.13, cover glass thickness 0.17, DIC), with a 488-nm laser and a 562-nm laser source for excitation. Lower laser intensity was used to avoid photo bleaching. Each slide was examined under reduced transmitted-light illumination; the area containing undamaged epithelium with underlying vasculature was chosen for analyses.

qPCR analysis. The levels of mRNA encoding *Atp7a* and *Atp7b* were quantified using qPCR. In short, the total RNA was isolated from brain capillaries, choroid plexus, RBE4, or Z310 cells using TRIzol reagent following the manufacturer's direction. An aliquot of RNA (1 μg) was reverse-transcribed into cDNA using the Bio-Rad iScript cDNA synthesis kit. The iTaq Universal SYBR Green Supermix (Bio-Rad) was used for qPCR analyses. The amplification was run in the CFX Connect Real-Time PCR Detection system (Bio-Rad) with an initial 3-min denaturation at 95°C; the amplification program was followed by 40 cycles of 30-s denaturation at 95°C, 10-s gradient 55.0°C–65.0°C and 30-s extension at 72°C. A dissociation curve was used to verify that the majority of fluorescence detected was attributed to the labeling of specific PCR products, and also to verify the absence of primer dimers and sample contamination. Each qPCR reaction was run in triplicate. Relative gene mRNA expression ratios between groups were calculated using the ΔΔCt formulation where Ct is the threshold cycle time value. The Ct values of interested genes were first normalized with that of glyceraldehyde-3-phosphate dehydrogenase (*Gapdh*) in the same sample to obtain the ΔΔCt values, and then relative ratios between control and treatment groups were calculated and expressed as relative gene expression by setting the control as 100% (Livak and Schmittgen, 2001). The amplification efficiencies of target genes and the internal reference were examined by determining the variations of the Ct with a series of control template dilutions.

The forward and reverse primers for *Atp7a* and *Atp7b* genes were designed using Primer Express 3.0 software. The primer sequences for rat *Atp7a* used in this study were: forward primer 5′-CCT CAA CAG CGT CGT CAC TA-3′ and reverse primer 5′-GAC TAG CAG CAT CCC CAA AG-3′ (GenBank Accession No. NM_052803.1), and for *Atp7b*, the forward primer 5′-GTC ACA CCC TGC TTG GAT TT-3′ and reverse primer 5′-CCT GAT GGG CCT ATT TCT CA-3′ (GenBank Accession No. NM_012511.2). The rat *Gapdh* used as an internal control had a forward primer 5′-CCT GGA GAA ACC TGC CAA GTAT-3′ and a reverse primer 5′-AGC CCA GGA TGC CCT TTA GT-3′ (GenBank Accession No. NM_017008).

Western blot analysis. Total cellular proteins from control and Mn-treated brain capillaries, choroid plexus tissues, RBE4 and Z310 cells were extracted in a homogenization buffer containing 20mM Tris (pH 7.5), 5mM EGTA, 1% Triton X-100, 0.1% SDS, and the protease inhibitor cocktail (Calbiochem, CA). Samples were sonicated, centrifuged, and quantified for protein concentrations using the Bradford assay. Protein samples were mixed with 2× Laemmli sample buffer (Bio-Rad) and boiled for 5 min. Samples were then loaded on the 8 + 15% dual-layer tris-glycine SDS-polyacrylamide gels, electrophoresed and transferred to a PVDF membranes. The membranes were blocked with 5% dry milk (fat free) in Tris-buffered saline with 0.1% Tween 20 (TBST) and incubated overnight at 4°C with the primary polyclonal antirabbit ATP7A or ATP7B antibodies (1:100), followed by the staining with a horseradish-peroxidase-conjugated goat antirabbit IgG antibody (1:3000) at room temperature for 1 h. PVDF membranes were developed using ECL Western Blotting Substrate and the Bio-Rad Molecular Imager (ChemiDoc XRS+ with Image Lab Software). β-Actin (42 kDa) was used as an internal control. The band intensity was quantified using ImageJ and reported in optical density (OD).

ATP7A or ATP7B siRNA knockdown studies. Silencer select predesigned *Atp7a* (Cat. no. s128720), *Atp7b* (Cat. no. s127497) and negative control no. 1 siRNA (Cat. no. 4390844) were purchased from Ambion (Life Technologies). The sense and antisense sequences of *Atp7a* siRNA were 5′-CAG UCA AGA GGA UUC GAA Utt-3′ and 5′-AUU CGA AUC CUC UUG ACU Gtt-3′ (length: 21 bp, G/C%: 38%), respectively. The sense and antisense sequences of *Atp7b* siRNA were 5′-CAU AGA AUC UAA GCU CAC Att-3′ and 5′-UGU GAG CUU AGA UUC UAU Gtt-3′ (length: 21 bp, G/C%: 33%), respectively. The transfection reagent lipofectamine RNAiMAX (Cat. no. 13778-075), a newly released product from Life Technologies, was found to work best in RBE4 and Z310 cells after a series of preliminary screenings. Transfection conditions were optimized according to the following variables: initial seeding density, volume of transfection reagent, duration of transfection, and concentration of siRNA.

RBE4 and Z310 cells were seeded at a density of 3×10^5 cells/well in six-well plates and allowed to grow for 24 h to achieve 50% confluence. siRNA transfection systems were then prepared as following: (1) 0.5 μl lipofectamine RNAiMAX was diluted in 100 μl OPTI-MEM medium (Life Technologies) and incubated for 10 min at room temperature; (2) *Atp7a* siRNA were diluted in separate tubes with 100 μl OPTI-MEM medium to the final concentrations of 20, 40, and 80 nM/well; (3) *Atp7b* siRNA were diluted in separate tubes with 100 μl OPTI-MEM medium to the final concentrations of 40 and 80 nM/well; and (4) negative control siRNA were diluted in separate tubes with 100 μl OPTI-MEM medium to the final concentrations of 20, 40, and 80 nM/well. The RNAiMAX and siRNA working solutions were mixed and incubated at room tempera-

ture for 15 min. The original cell culture medium was removed; after three washes with PBS, the medium was replaced with 200 μl RNAiMAX and siRNA mixed working solution along with 800 μl OPTI-MEM medium to obtain a total volume of 1 ml medium/well. The cell cultures were placed into the 37°C incubator for 8 h. An additional 1 ml of prewarmed regular cell growth medium was then added to each well and cells were allowed to grow up to 48 h. The knockdown effect was verified using qPCR and Western blot.

Cellular ^{64}Cu retention studies. RBE4 and Z310 cells were seeded in the 24-well plates at a density of 5×10^4 cells/well, allowed to grow for 24 h to achieve 30% confluence, and then randomly divided into seven groups for various treatments for 48 h: (1) the control group without any treatment; (2) the negative control group treated with negative control siRNA; (3) the Mn-exposed group with 100μM $MnCl_2$; (4) the 80nM *Atp7a* siRNA knockdown group; (5) the cotreatment group with 100μM $MnCl_2$ and 80nM *Atp7a* siRNA transfection; (6) the 40nM *Atp7b* siRNA knockdown group; and (7) the cotreatment group with 100μM $MnCl_2$ and 40nM *Atp7b* siRNA transfection.

At the end of treatments, cells were incubated with a mixture working solution containing 5μM $CuCl_2$ and ^{64}Cu (specific activity 5 μCi/ml) in HBSS for 1, 2, 4, 8, 12, and 24 h followed by three washes with PBS to remove excess $^{64}CuCl_2$, and then harvested in 0.2 ml double-deionized water. The precipitated cell pellet representing intracellular $^{64}CuCl_2$ radioactivity was counted using a Perkin-Elmer Wizard-1480 Gamma-counter (Shelton, CT). Thereafter, the total proteins were quantified using the Bradford Assay. The radioactivity of ^{64}Cu was normalized by total protein concentration and results were expressed as ^{64}Cu DPM/μg protein.

Two-chamber Transwell ^{64}Cu transport study using primary culture of choroidal epithelial cells. The two-chamber Transwell transport system has been extensively used in our transport research (Crossgrove *et al.*, 2005; Monnot and Zheng, 2012; Shi and Zheng, 2005; Wang *et al.*, 2008b). To prepare primary choroidal epithelial cells, 4-week-old rats were sacrificed to harvest plexus tissues. These tissues were digested in HBSS containing 0.2% pronase at 37°C for 10–15 min, followed by two washes with HBSS, and then resuspended in growth DMEM medium containing 10% FBS, 100 U/ml penicillin, 100 μg/ml streptomycin, 0.25 μg/ml amphotericin, 100 μg/ml gentamicin, and 10 ng/ml EGF. A 20-gauge needle was used to pass cells through the needle 14–15 times to ensure adequate cell separation for seeding. Cells stained with 0.4% Trypan blue were counted under a light microscope to determine the cell number; cells were then seeded on 35-mm Petri dishes (precoated with collagen) at a density of (2–3) $\times 10^5$ cells/ml. The cultured cells were maintained at 37°C with 95% air-5% CO_2 in a humidified incubator without disturbance for at least 48 h. The growth medium was replaced 3 days after the initial seeding and every 2 days thereafter.

After cultured in dishes for 7–10 days, the cells were transferred to the inner chamber of the Transwell transport device. The inner chamber, also known as the apical chamber, was immersed in the outer chamber. An aliquot of 0.8-ml cell suspension (10×10^5 cells/ml for initial seeding) was added to the inner chamber and 1.2 ml of medium was added to the outer chamber. The transepithelial electrical resistance (TEER), an indicator of the tightness of the barrier, was used to track the formation of a cellular monolayer between the inner and outer chambers. The TEER value was measured every other day using an Epithelial Volt-Ohmmeter (EVOM, World Precision Instruments, Sarasota, FL) until the resistance reached 50–60 Ω cm^2. The same two-chamber system without cells was used as blank, and the background was subtracted from the measured TEER. When cells grew to confluence, the surface level of the medium in the inner chamber was roughly 2 mm above the outer chamber.

When a confluent cell monolayer was formed, the primary culture was divided into seven groups of similar TEER value for the same treatment manner as described in the section of cellular ^{64}Cu retention studies. At the end of treatments, an aliquot of $^{64}CuCl_2$ mixed with space marker ^{14}C-sucrose was prepared to a final concentration of 5μM $CuCl_2$ (specific activity 5 μCi/ml) and ^{14}C-sucrose (specific activity 0.5 μCi/ml) in HBSS. A total volume of 0.8 ml ^{64}Cu-containing medium was added to each inner chamber (donor) for the efflux study. A series of time points (0, 5, 10, 15, 30, 60, 90 min, and 2, 3, and 4 h) were set for sample collection. At each time point, 10 μl of medium was collected from both chambers and replaced with an equal volume of the counterpart working medium. All samples were counted by an auto-Gamma 5000 Series Gamma Counter. To count ^{14}C-sucrose, the samples were mixed with Eco-lite cocktail and counted on a Packard Tr-Carb 2900 TR Liquid Scintillation Analyzer.

To determine the transport coefficient for ^{64}Cu and ^{14}C-sucrose across the monolayer, the data within the linear range were used for linear regression analyses. The slope (DPM/ml/min) of each dataset was used to calculate the influx and efflux (permeability) coefficients of ^{64}Cu when they were added in the outer or inner chamber, respectfully, using the equation (3):

$$P_T \text{ or } P_B = \frac{V_R}{A \times C_D} \times \frac{\Delta C_R}{\Delta t} \quad (3)$$

where P_T, total (cell monolayer + membrane) permeability coefficient (cm/min); P_B, blank permeability coefficient (cm/min); V_R, volume of the receiver (ml or cm^3); A, surface area of transport membrane in the inner chamber (cm^2); C_D, concentration in donor chamber (mg/ml); and $\Delta C_R/\Delta t$, changes of concentration in the receiver over a fixed time period (mg/ml/min). Thus, the permeability or flux coefficient of metals (P_E) can be

obtained from the equation (4) (Monnot *et al.*, 2011; Shi and Zheng, 2005; Wang *et al.*, 2008b):

$$\frac{1}{P_E} = \frac{1}{P_T} - \frac{1}{P_B} \quad (4)$$

where P_E is the permeability coefficient of epithelial barrier.

Statistics analysis. All data are expressed as mean ± SD; statistical analyses of the differences between groups were carried out by one-way ANOVA with *post hoc* comparisons by the Dunnett's test or Student's *t*-tests using SPSS for Windows (version 20.0). The differences between two means were considered significant if *p*-values were equal or less than 0.05.

RESULTS

Part 1: BBB Studies

Expression of ATP7A and ATP7B in the BBB. Both ATP7A and ATP7B have been found in brain capillary endothelia (Choi and Zheng, 2009; Qian *et al.*, 1998). However, the relative abundance of their expression in the BBB was unclear. Thus, the purpose of this experiment was to compare expression levels of *Atp7a* and *Atp7b* in brain capillary endothelia and RBE4 cells. By normalizing with the housekeeping gene *Gapdh*, our data confirmed the presence of both Cu-ATPases in brain capillaries and RBE4 cells; further, we found that the mRNA expression level of *Atp7a* in brain capillaries and RBE4 cells were 12.8- and 4.8-fold higher than those of *Atp7b* ($p < 0.01$), respectively (Fig. 1).

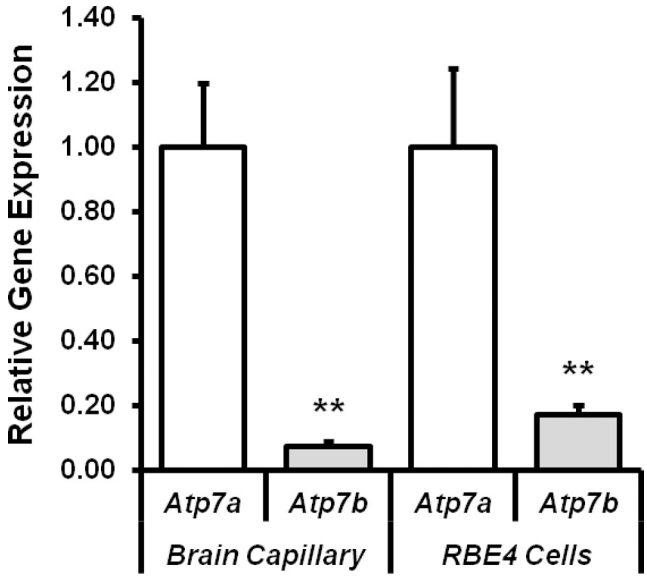

FIG. 1. Comparison of *Atp7a* and *Atp7b* mRNA expression levels in control brain capillaries and RBE4 cells. Relative mRNA levels of *Atp7a* and *Atp7b* in control brain capillaries and RBE4 cells were quantified by qPCR and expressed as the ratios of *Atp7a*/*Gapdh* or *Atp7b*/*Gapdh*. The data are representative of triplicate experiments. Data represent mean ± SD, $n = 5$–6; $^{**}p < 0.01$.

Decreased expression of ATP7A and ATP7B in brain capillaries and RBE4 cells following Mn exposure. Because both ATP7A and ATP7B play pivotal roles in regulating Cu transport by the BBB, the alteration in expression of both transporters may contribute to Mn-induced imbalance of Cu homeostasis in brain (Zheng *et al.*, 2009). To determine whether Mn exposure affects the expression of Cu-ATPases, we used qPCR and Western blot to quantify mRNA and protein expression levels of ATP7A and ATP7B in brain capillaries of rats subchronically exposed to Mn at 6 mg/kg once daily for 4 weeks. Data in Figure 2(I)A and B indicated that expressions of *Atp7a* and *Atp7b* mRNA levels in brain capillaries were significantly decreased by 34 and 44%, respectively, as compared with controls ($p < 0.05$). The Western blot analyses confirmed that *Atp7a* and *Atp7b* protein levels in brain capillaries were reduced by 50 and 22% of the control ($p < 0.01$), respectively, following Mn exposure (Figs. 2(I)C–F). It became clear that Mn-induced alteration of brain Cu homeostasis may be associated with Mn effect on Cu transport in brain capillary endothelia.

We further conducted a time-course study using the immortalized rat brain endothelial cell line RBE4. Data showed that the reduction of *Atp7a* and *Atp7b* mRNA levels appeared as early as 12 h following exposure to 100μM $MnCl_2$, and the effect remained at 24 and 48 h of Mn treatment (Figs. 2(II)A and B). The Western blot analyses confirmed the significant time-dependent inhibition of ATP7A and ATP7B following Mn exposure in BBB cells *in vitro* ($p < 0.01$) (Figs. 2(II)C–F).

In control, untreated cells, the confocal images revealed that the fluorescent signals of ATP7A or ATP7B were mainly president in the cytosol surrounding the nuclei (Figs. 3A-a and 3B-a). Following 24-h treatment with 100μM $MnCl_2$, both ATP7A and ATP7B fluorescent signal intensities in RBE4 cells were visibly weakened as compared with controls (Figs. 3A-d and 3B-d).

Increase in brain regional Cu levels following in vivo *subchronic Mn exposure.* We used AAS to determine Mn and Cu levels in selected brain regions. Data presented in Table 1 revealed that the Mn levels in all dissected brain regions were significantly increased in Mn-exposed animals, as compared with controls ($p < 0.01$). The Cu concentration in the striatum of Mn-exposed rats (4.73 ± 0.94 μg/g tissue) was 2.2-fold higher than that of controls (2.18 ± 0.54 μg/g tissue, $p < 0.05$). In addition, the Cu concentration in the frontal cortex (2.82 ± 0.31 μg/g tissue) following Mn exposure showed a trend of increase, although not statistically significant, as compared with the control (1.97 ± 0.52 μg/g tissue). These *in vivo* data support the finding that Mn exposure alters brain Cu homeostasis.

To study Cu transport by the BBB, we used the *in situ* brain perfusion technique to determine the Cu uptake by brain capil-

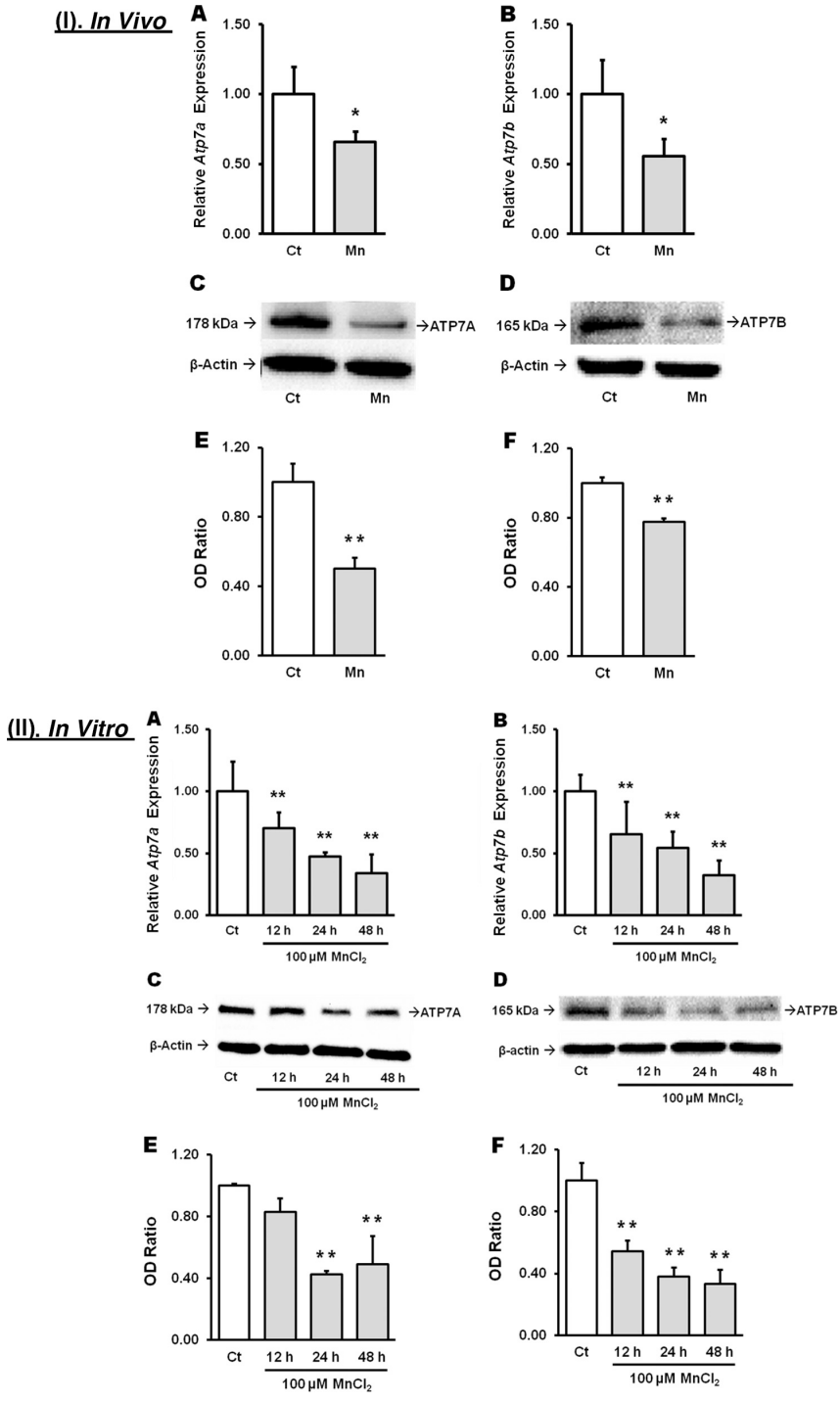

FIG. 2. Decrease in mRNA and protein expression levels of ATP7A and ATP7B in the *in vivo* brain capillary and *in vitro* RBE4 cells following Mn exposure. (I) *In vivo* subchronic exposure study: rats received either daily ip injection of 6 mg Mn/kg or saline (as control), 5 days per week, for 4 weeks. (A and B) *Atp7a* and *Atp7b* mRNA expression levels in the brain capillary were quantified by qPCR and expressed as the ratios of *Atp7a*/*Gapdh* or *Atp7b*/*Gapdh*. The data are representative of triplicate experiments. Data represent mean ± SD, $n = 5$; $*p < 0.05$, as compared with controls. (C and D). Representative Western blot autographs of *Atp7a* and *Atp7b* in the brain capillary. (E and F). Quantification of Western blot densitometry and statistical analysis. Ct: control group; Mn: Mn-exposed group. Data represent mean ± SD, $n = 3$; $**p < 0.01$, as compared with controls. (II) *In vitro* studies with RBE4 cells: (A and B) *Atp7a* and *Atp7b* mRNA expression levels in RBE4 cells were quantified by qPCR and expressed as the ratios of *Atp7a*/*Gapdh* or *Atp7b*/*Gapdh*. The data are representative of triplicate experiments. Data represent mean ± SD, $n = 6$; $**p < 0.01$, as compared with controls. (C and D) Representative Western blot autographs of *Atp7a* and *Atp7b* in RBE4 cells. (E and F) Quantification of Western blot densitometry and statistical analysis. Ct: control group; Mn: Mn-exposed group. Data represent mean ± SD, $n = 3$; $**p < 0.01$, as compared with controls.

TABLE 1
Mn and Cu Concentrations in Hippocampus, Striatum, and Frontal Cortex Following *in vivo* Subchronic Mn Exposure

Group	HP (μg/g tissue)		ST (μg/g tissue)		FC (μg/g tissue)	
	Mn	Cu	Mn	Cu	Mn	Cu
Ct	0.97 ± 0.29	2.67 ± 0.76	0.42 ± 0.05	2.18 ± 0.28	0.43 ± 0.03	1.97 ± 0.52
Mn-E	1.82 ± 0.30**	2.29 ± 0.52	2.87 ± 0.71**	4.73 ± 0.54*	3.40 ± 0.93**	2.82 ± 0.31

Note. Rats received 6 mg Mn/kg once daily for 4 weeks. Concentrations of Cu and Mn were determined by AAS. Data represent mean ± SD, $n = 6$. HP, ST, FC, Ct, and Mn-E represent hippocampus, striatum, frontal cortex, control, and Mn-exposed groups, respectively.
*$p < 0.05$, as compared with the control.
**$p < 0.01$, as compared with the control.

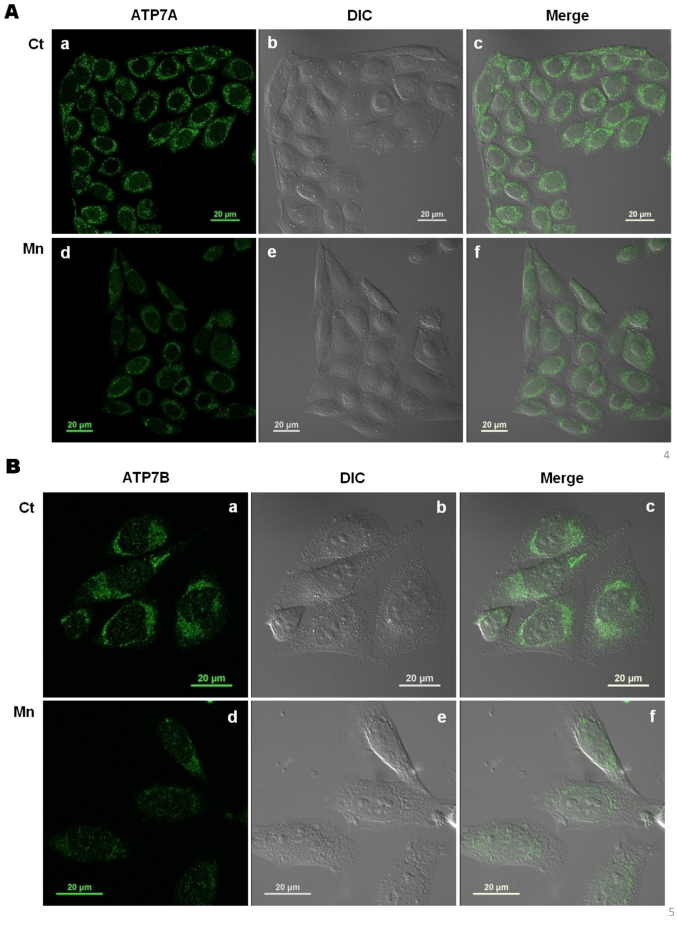

FIG. 3. Subcellular distribution of ATP7A and ATP7B in RBE4 cells following *in vitro* Mn exposure. (A) ATP7A localization in RBE4 cells. (a and d) ATP7A fluorescent signals; (b and e) DIC images; (c and f) merged images. (B) ATP7B localization in RBE4 cells. (a and d) ATP7B fluorescent signals; (b and e) DIC images; (c and f) merged images.

laries, parenchyma, choroid plexus, and CSF. Data in Table 2 showed that in control animals, the highest uptake of ^{64}Cu was in the choroid plexus (8.49 ml/g), followed by in a descending order, brain parenchyma (0.200–0.337 ml/g), brain capillaries (0.066–0.201 ml/g), and CSF (0.038 ml/g). The same descending order was also observed in Mn-exposed animals. The V_d of ^{64}Cu entering choroid plexus was about 220-fold greater than that of ^{64}Cu entering the CSF in control animals, and this ratio was increased to 370 folds in Mn-exposed animals, suggesting that the choroid plexus sequestered an extraordinary amount of Cu from the blood and Mn exposure further enhanced this capacity. The large concentration gradient of Cu between the choroid plexus and CSF suggested a remarkably restricted regulation of Cu transport into the CSF via the BCB. Hence, the elevation of CSF V_d in Mn-exposed animals could be due to the increase in Cu exchange between the brain interstitial fluid and CSF or to the lesser extent the elevated release of Cu from the choroid plexus to the CSF under Mn influences.

A three-fold increase in the uptake of ^{64}Cu by the capillary-depleted brain parenchyma in selected regions, i.e., HP, ST, and FC was found following subchronic Mn exposure, when compared with the control ($p < 0.01$) (Table 2). In both control and Mn-exposed groups, V_d values of ^{64}Cu distributing in brain capillaries were generally lower than those in capillary-depleted brain parenchyma, indicating that Cu ions were readily transported into the brain parenchyma, but not accumulated in the cerebral capillary.

By calculating the unidirectional uptake rate (K_{in}) in control brain parenchyma and capillary, which is corrected by V_d of ^{14}C-sucrose, the K_{in} values were about 1.7–3.0-fold lower in capillary (0.55–1.67 μl/s/g) than in brain parenchyma (1.67–2.81 μl/s/g) (Table 2). Mn *in vivo* exposure significantly increased the K_{in} rate to each regional capillary and parenchyma, but did not change the differential uptake rates between capillary and parenchyma. Noticeably, there was no significant difference in the ^{14}C-sucrose uptake by the CSF, choroid plexus, brain parenchyma, and capillaries in control and Mn-exposed animals (Table 3), suggesting that there was no structural leakage of the BBB in the Mn-exposed animals. Combining V_d and K_{in} data, it seemed likely that the main entry of Cu into the brain was via the blood-BBB route.

Cellular ^{64}Cu retention in RBE4 cells following in vitro *Mn exposure and siRNA knockdown.* ATP7A and ATP7B are responsible for exporting excess Cu ions out of the cells. A decreased expression of both Cu transporters would lead to cellular accumulation of Cu. To test this hypothesis, we used siRNA

TABLE 2
Brain Regional ^{64}Cu Uptake Following *in vivo* Subchronic Mn Exposure

Brain region		V_d of ^{64}Cu (ml/g)		K_{in} of ^{64}Cu (μl/s/g)	
		Ct	Mn-E	Ct	Mn-E
CSF		0.038 ± 0.019	0.084 ± 0.049*	0.316 ± 0.155	0.702 ± 0.412*
CP		8.490 ± 3.830	14.06 ± 3.14*	70.71 ± 31.88	117.0 ± 26.13*
Parenchyma	HP	0.257 ± 0.061	0.694 ± 0.149**	2.14 ± 0.51	5.78 ± 1.24**
	ST	0.200 ± 0.066	0.667 ± 0.146**	1.67 ± 0.55	5.56 ± 1.21**
	FC	0.337 ± 0.105	0.932 ± 0.338**	2.81 ± 0.87	7.76 ± 2.81**
Capillary	HP	0.156 ± 0.041	0.412 ± 0.226*	1.30 ± 0.34	3.44 ± 1.88*
	ST	0.066 ± 0.015	0.144 ± 0.032**	0.55 ± 0.13	1.20 ± 0.26**
	FC	0.201 ± 0.127	0.797 ± 0.490*	1.67 ± 1.05	6.64 ± 4.09*

Note. Data represent mean ± SD, $n = 4$–8. CSF, CP, HP, ST, FC, Ct, and Mn-E represent cerebrospinal fluid, choroid plexus, hippocampus, striatum, frontal cortex, control, and Mn-exposed groups, respectively.
*$p < 0.05$, as compared with the control.
**$p < 0.01$, as compared with the control.

TABLE 3
Brain Regional ^{14}C-Sucrose Uptake Following *in vivo* Subchronic Mn Exposure

Brain region		V_d of ^{14}C-sucrose (ml/g)		K_{in} of ^{14}C-sucrose (μl/s/g)	
		Ct	Mn-E	Ct	Mn-E
CSF		0.010 ± 0.006	0.014 ± 0.007	0.083 ± 0.051	0.116 ± 0.059
CP		0.119 ± 0.064	0.126 ± 0.047	0.990 ± 0.533	1.050 ± 0.395
Parenchyma	HP	0.004 ± 0.002	0.004 ± 0.001	0.036 ± 0.016	0.033 ± 0.010
	ST	0.003 ± 0.001	0.004 ± 0.002	0.026 ± 0.006	0.037 ± 0.017
	FC	0.003 ± 0.001	0.003 ± 0.001	0.022 ± 0.011	0.026 ± 0.010
Capillary	HP	0.007 ± 0.002	0.007 ± 0.002	0.057 ± 0.020	0.062 ± 0.013
	ST	0.007 ± 0.002	0.007 ± 0.002	0.061 ± 0.018	0.056 ± 0.013
	FC	0.006 ± 0.003	0.005 ± 0.002	0.054 ± 0.021	0.046 ± 0.013

Note. Data represent mean ± SD, $n = 4$–8. CSF, CP, HP, ST, FC, Ct, and Mn-E represent cerebrospinal fluid, choroid plexus, hippocampus, striatum, frontal cortex, control, and Mn-exposed groups, respectively.

to specifically knockdown the expression of *Atp7a* and *Atp7b* and then to study cellular Cu retention. Our data showed that introductions of 80nM *Atp7a* and 40nM *Atp7b* siRNA for 48 h resulted in 86 and 50% reductions of *Atp7a* and *Atp7b* mRNA levels, respectively, as compared with the control ($p < 0.01$, Supplementary figs. 1A and B). The Western blot results further confirmed a significant knockdown of ATP7A (83% at 80nM *Atp7a* siRNA) and ATP7B (57% at 40nM *Atp7b* siRNA) protein levels ($p < 0.01$, Supplementary figs. 1C–F).

Once the effective condition for siRNA transfection was established, we performed the ^{64}Cu retention experiment in Mn treated- or siRNA transfected-RBE4 cells with 5μM $CuCl_2$ and ^{64}Cu (specific activity: 5 μCi/ml) for 1, 2, 4, 8, 12, and 24 h. In the presence of 100μM $MnCl_2$, cellular ^{64}Cu levels were significantly higher than those of the regular control following 2, 4, 8, 12, and 24 h incubations with ^{64}Cu ($p < 0.01$); in *Atp7a*- or *Atp7b*-knockdown cells, the cellular ^{64}Cu retention levels were lower than those of the negative siRNA control during the incubation time points of 1, 2, and 4 h, but significantly increased about 5.9 ($p < 0.01$) and 6.2 folds ($p < 0.05$) in 12 h-incubated cells, respectively, as compared with the negative siRNA control (Table 4). When *Atp7a* and *Atp7b*-knockdown cells were further exposed to Mn, significantly elevated cellular ^{64}Cu retention was observed following 2, 4, 8, 12, and 24 h incubations, as compared with the regular ($p < 0.01$), and negative siRNA control ($p < 0.05$); in addition, the cotreatment groups with Mn and siRNAs apparently have more ^{64}Cu retained in RBE4 cells in comparison with siRNA knockdown groups ($p < 0.01$) (Table 4). As compared with Mn-E group, *Atp7a* and *Atp7b*-knockdown cells were observed with significantly less ^{64}Cu retention following 1, 2, and 4 h incubations ($p < 0.01$), whereas higher intracellular ^{64}Cu levels were detected following 12 and 24 h incubations ($p < 0.05$) (Table 4). The highest cellular ^{64}Cu level was 1095 DPM/μg protein in Mn- and *Atp7b*-treated cells with 24 h ^{64}Cu incubation. Thus, Mn-

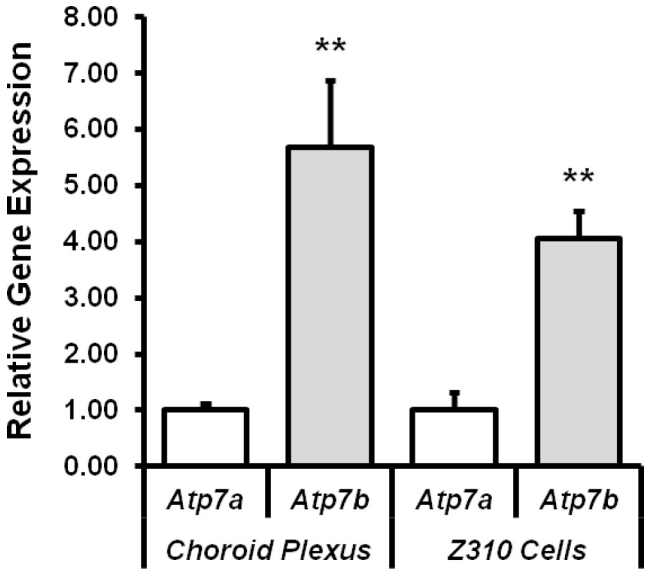

FIG. 4. Comparison of *Atp7a* and *Atp7b* mRNA expression levels in freshly isolated choroid plexus tissues and choroidal Z310 cells. Relative mRNA levels of *Atp7a* and *Atp7b* in the control choroid plexus and Z310 cells were quantified by qPCR and expressed as the ratios of *Atp7a*/*Gapdh* or *Atp7b*/*Gapdh*. The data are representative of triplicate experiments. Data represent mean ± SD, $n = 5$–6; $^{**}p < 0.01$.

induced reduction of ATP7A and ATP7B may lead to the cell's failure to expel intracellular Cu.

Part 2: BCB Studies

Comparison of ATP7A and ATP7B in the BCB. We used the same technical approaches as described in Part 1: BBB studies to study the expression of *Atp7a* and *Atp7b* in the freshly isolated choroid plexus tissues and in an immortalized choroidal epithelial Z310 cell line. Data in Figure 4 revealed that both ATP7A and ATP7B existed in choroid plexus tissues and choroidal Z310 cells. In contrast to the results in BBB, the expressions of *Atp7a* mRNA in plexus tissues and Z310 cells were 4.7- and 3.1-fold lower than those of *Atp7b* ($p < 0.01$). Thus, it seems likely that ATP7B and ATP7A may play functionally different roles in regulating Cu transport across the BCB and BBB.

Decreased expression of ATP7A and ATP7B in choroid plexus tissues and choroidal Z310 cells following Mn exposure. We used qPCR and Western blot to determine the expression levels of *Atp7a* and *Atp7b* in the choroid plexus of rats and Z310 cells with or without Mn exposure. Following *in vivo* subchronic Mn exposure, *Atp7a* and *Atp7b* mRNA levels normalized by housekeeping gene *Gapdh* were significantly decreased by 37% ($p < 0.01$) and 38% ($p < 0.05$), respectively, as compared with the controls (Figs. 5(I)A and B). The Western blot analyses showed that the protein expression levels of *Atp7a* and *Atp7b* in plexus tissues of Mn-exposed animals were reduced by 39% ($p < 0.01$) and 35% ($p < 0.05$) of the control, respectively (Figs. 5(I)C–F).

In the *in vitro* time-course study, it was evident that the reduction of *Atp7a* and *Atp7b* mRNA took place as early as 12 h following 100μM Mn exposure ($p < 0.01$) (Figs. 5(II)A and B). Western blot analyses demonstrated that exposure to 100μM $MnCl_2$ for 12, 24, and 48 h resulted in decreased protein expression levels of *Atp7a* (39, 54, and 55% reduction, respectively, $p < 0.01$) and *Atp7b* (29, 59, and 64% reduction, respectively, $p < 0.01$) (Figs. 5(II)C–F). Thus, our *in vitro* data supported an inhibitory effect of Mn on expressions of ATP7A and ATP7B in choroid epithelial cells.

Subcellular trafficking ATP7A and ATP7B in choroid plexus tissues following in vitro *Cu incubation.* The epithelial cells in the choroid plexus are highly polarized with the apical microvilli facing the CSF and the basolateral membrane facing the blood. Because ATP7A and ATP7B function to expel Cu out of the cell, the direction to which these Cu transporters transport Cu, either toward the blood or CSF, is essential to the understanding of how the BCB regulates the Cu homeostasis in the CSF. This set of experiments was designed to understand the intracellular trafficking of both Cu-ATPases by using the freshly dissected choroid plexus tissues. Under the baseline condition without addition of Cu, both ATP7A- and ATP7B-associated fluorescent signals were mainly seen in the perinuclear region of the choroidal epithelia (Figs. 6A-a and 6B-a). In the presence of 5 or 50μM $CuCl_2$, the ATP7A signals in the choroid plexus were translocated toward the apical microvilli (Figs. 6A-d and g). In contrast, the ATP7B fluorescent signals were moved, in the opposite direction, toward the basolateral membrane (Figs. 6B-d and g). These image evidences appeared to suggest that when the cellular Cu level was increased in the choroidal epithelia, ATP7A acted to expel excess Cu ions from the cytosol toward the apical CSF compartment, whereas ATP7B functioned to excrete extra Cu ions from the cytoplasm to the basolateral blood compartment. Because ATP7B expression level was higher than ATP7A in the BCB (Fig. 4), it was reasonable to postulate that the choroid plexus may favor the Cu efflux from the CSF to blood.

To verify Mn effect on the trafficking pattern of ATP7A and ATP7B, we used the same *in vivo* Mn exposure regimen as described in Part 1 BBB studies to examine the intracellular distribution of proteins by the confocal microscopy. Results in Figure 6C showed that after *in vivo* Mn exposure the ATP7A signals were visibly concentrated in the choroidal microvilli; little was seen in the perinuclear region (Figs. 6C-d and f). It was also noticed that the ATP7A fluorescent intensities were weaker in Mn-exposed animals than those in controls (Figs. 6C-d vs. 7C-a). In contrast, the ATP7B fluorescent signals in choroid plexus tissues following *in vivo* Mn exposure were concentrated mainly in the basolateral membrane (Figs. 6D-d and f). The weakened ATP7B signals were also observed in plexus tissues of Mn-exposed animals (Figs. 6D-d vs. 6D-a). The data appeared to indicate that Mn exposure stimulated the subcellular translocation of ATP7A from the cytosol toward the apical microvilli; in

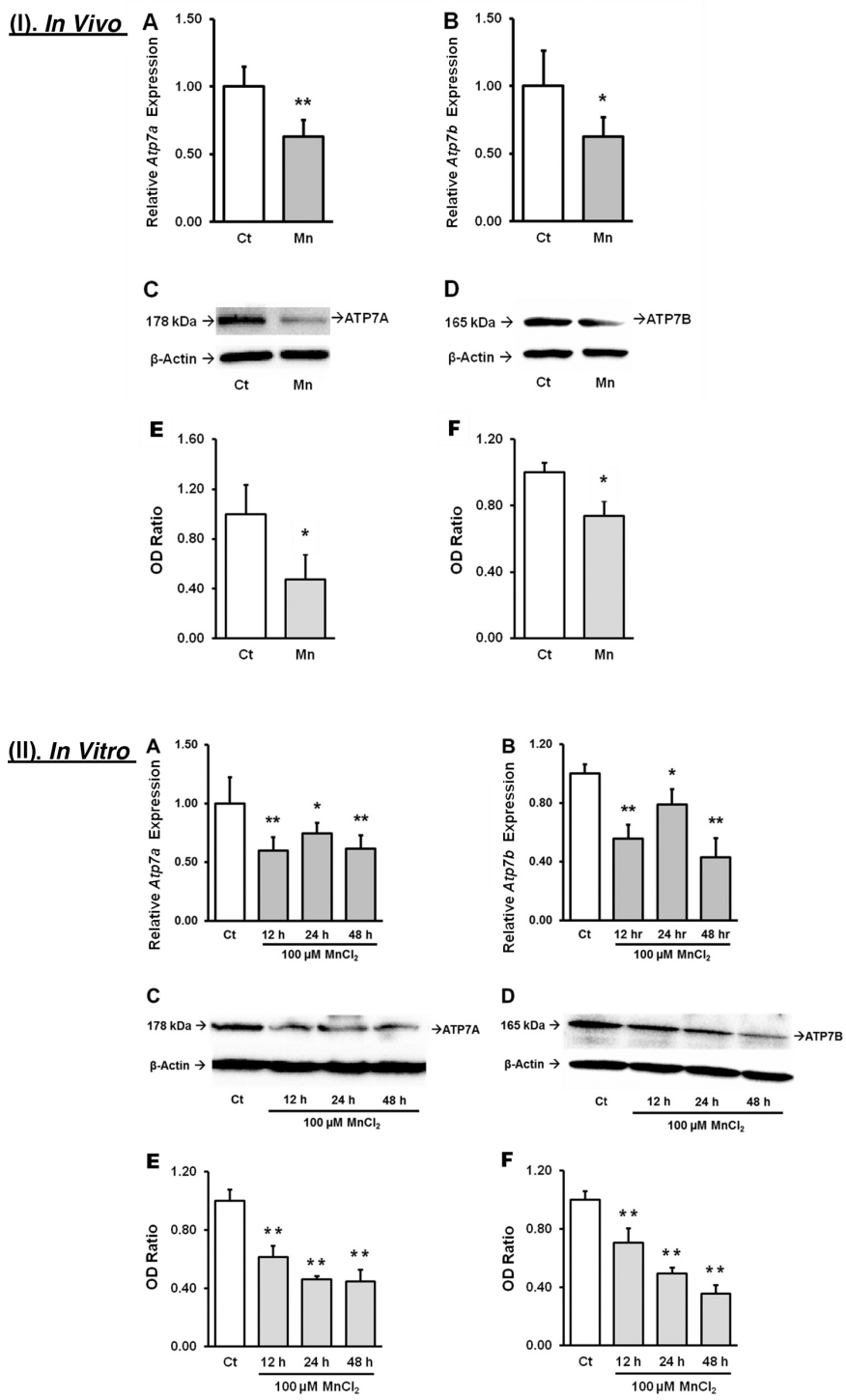

FIG. 5. Decreased mRNA and protein levels of ATP7A and ATP7B in the *in vivo* choroid plexus tissues and *in vitro* choroidal Z310 cells following Mn exposure. (I) *In vivo* subchronic exposure study: (A and B) *Atp7a* and *Atp7b* mRNA expression levels in the choroid plexus were quantified by qPCR and expressed as the ratios of *Atp7a*/*Gapdh* or *Atp7b*/*Gapdh*. The data are representative of triplicate experiments. Data represent mean ± SD, $n = 6$; $*p < 0.05$, $**p < 0.01$ as compared with controls. (C and D) Representative Western blot autographs of *Atp7a* and *Atp7b* in plexus tissues. (E and F) Quantification of Western blot densitometry and statistical analysis. Ct: control group; Mn: Mn-exposed group. Data represent mean ± SD, $n = 3$; $*p < 0.05$, as compared with controls. (II) *In vitro* studies with Z310 cells: (A and B) Relative mRNA levels of *Atp7a* and *Atp7b* were quantified by qPCR and expressed as the ratios of *Atp7a*/*Gapdh* or *Atp7b*/*Gapdh*. The data are representative of triplicate experiments. Data represent mean ± SD, $n = 6$; $*p < 0.05$, $**p < 0.01$, as compared with controls. (C and D) Representative Western blot autographs of ATP7A and ATP7B in Z310 cells. (E and F) Quantification of Western blot densitometry and statistical analysis. Ct: control group; Mn: Mn-exposed group. Data represent mean ± SD, $n = 3$; $**p < 0.01$, as compared with controls.

TABLE 4
Intracellular ^{64}Cu Retention (DPM/μg Protein) in RBE4 Cells Following Mn Exposure or siRNA Knockdown

Group	Time point (h)					
	1	2	4	8	12	24
Ct	37.7 ± 5.93	49.1 ± 6.57	64.8 ± 6.46	82.1 ± 13.8	164 ± 25.7	392 ± 75.3
NCt	42.0 ± 4.68	46.6 ± 6.24	80.9 ± 10.2	93.3 ± 13.4	124 ± 57.8	459 ± 46.8
Mn-E	42.2 ± 8.06	70.4 ± 11.6**	98.1 ± 6.94**	104 ± 26.1*	696 ± 51.7**	496 ± 56.0*
Atp7a siRNA	23.9 ± 2.59$^{\#\#,\Delta\Delta}$	35.2 ± 7.92$^{\#,\Delta\Delta}$	59.8 ± 14.9$^{\#,\Delta\Delta}$	125 ± 16.9$^{\#\#,\Delta}$	727 ± 97.0$^{\#\#,\Delta\Delta}$	540 ± 66.9
Atp7b siRNA	21.4 ± 3.97$^{\#\#,\Delta\Delta}$	38.2 ± 4.76$^{\Delta\Delta}$	53.7 ± 5.20$^{\#\#,\Delta\Delta}$	66.6 ± 10.0$^{\#\#,\Delta\Delta,\diamond\diamond}$	766 ± 69.8$^{\#\#,\Delta\Delta}$	618 ± 73.5$^{\#\#,\Delta}$
Mn + *Atp7a* siRNA	38.6 ± 3.24$^{\diamond\diamond}$	67.7 ± 9.07$^{**,\#\#,\diamond\diamond}$	104 ± 29.5$^{**,\#,\diamond\diamond}$	154 ± 6.55$^{**\#\#,\Delta\Delta,\diamond\diamond}$	731 ± 177$^{**,\#\#,\Delta\Delta}$	639 ± 41.9$^{**,\#\#,\Delta}$
Mn + *Atp7b* siRNA	49.2 ± 9.98$^{**,\#,\S\S}$	95.9 ± 14.8$^{**,\#\#,\Delta\Delta,\S\S}$	107 ± 22.2$^{**,\#\#,\S\S}$	134 ± 14.0$^{**\#\#,\Delta\Delta,\S\S}$	831 ± 154$^{**,\#\#,\Delta\Delta}$	1095 ± 197$^{**,\#\#,\Delta\Delta,\S\S}$

Note. Data represent mean ± SD, $n = 4$–9. Ct, NCt, and Mn-E represent control, negative siRNA control, and Mn-exposed groups, respectively.
$^{*}p < 0.05$, as compared with the control.
$^{**}p < 0.01$, as compared with the control.
$^{\#}p < 0.05$, as compared with the negative siRNA control.
$^{\#\#}p < 0.01$, as compared with the negative siRNA control.
$^{\Delta}p < 0.05$, as compared with the Mn-E group.
$^{\Delta\Delta}p < 0.01$, as compared with the Mn-E group.
$^{\diamond\diamond}p < 0.01$, as compared with the *Atp7a* siRNA group.
$^{\S\S}p < 0.01$, as compared with the *Atp7b* siRNA group.

the meantime, it caused ATP7B to move toward the basolateral membrane.

For *in vitro* studies, immunostaining with confocal microscopy revealed that choroidal Z310 cells expressed both ATP7A and ATP7B proteins in the perinuclear region (Figs. 7A-a and 7B-a). After cells were treated with 100μM $MnCl_2$ for 24 h, intensities of both ATP7A and ATP7B fluorescent signals were visibly decreased (Figs. 7A-d and 7B-d), as compared with control cells (Figs. 7A-a and 7B-a). These image data from Z310 cells were consistent with the aforementioned *in vivo* data.

Increase in Mn and Cu concentrations in the serum, CSF and choroid plexus tissues following in vivo *subchronic Mn exposure.* In the same *in vivo* Mn exposure animal model, the AAS analyses revealed that the concentrations of Mn in serum, CSF and choroid plexus tissues were significantly increased by 8-, 11- and 8-folds, respectively, in Mn-exposed animals in comparison to controls ($p < 0.01$) (Table 5). The Cu concentration was increased by about 40% in the serum of the Mn-exposed rats as compared with controls ($p < 0.05$). In addition, the Cu concentration in the choroid plexus was increased more than two fold in Mn-exposed animals than in controls ($p < 0.01$); the data were comparable to nearly two fold increase of Cu concentrations in the CSF of Mn-exposed animals ($p < 0.05$) (Table 5). These *in vivo* findings suggest a disordered Cu balance in the BCB following Mn exposure.

Reduced Cu clearance by the BCB following in vivo *subchronic Mn exposure.* Because the Cu concentration in the CSF is largely regulated by the BCB, we sought to test the hypothesis that a high accumulation of Mn in the choroid plexus may disturb the Cu efflux transport by the BCB. Thus, an *in situ* VC perfusion technique was used to investigate the efflux kinetics of Cu via the choroid plexus in animals subchronically exposed to Mn. In this experiment, ^{64}Cu along with a space marker ^{14}C-sucrose was infused into the lateral ventricle; the CSF outflow was collected from the cistern magna to determine the radioactivity. The lost radioactivity in the distance between the ventricle and cistern magna, after correcting for the diffusion factor by ^{14}C-sucrose, is considered to be transported by the choroid plexus efflux mechanism (Chodobski and Segal, 2005; Deane *et al.*, 2004). The time courses in control rats in Figures 8A and 8B suggested that the percentages of ^{64}Cu and ^{14}C-sucrose in the outflow of CSF reached a plateau in 30 min after the initiation of perfusion.

Following *in vivo* Mn exposure, almost 100% of ^{14}C-sucrose radioactivity was recovered at the steady state (30–60 min) (Fig. 8A), suggesting that the little account of the space marker ^{14}C-sucrose was taken up by the choroid plexus and thus there was no structural leakage in the BCB in Mn-treated animals. In contrast, a significantly higher percentage of ^{64}Cu was recovered from the CSF outflow in Mn-exposed animals as compared with controls (Fig. 8B). A higher percentage of ^{64}Cu recovered from the CSF outflow implied a lower *in vivo* uptake of Cu molecules by the choroid plexus.

The data from the last five time points were then used to calculate the steady-state percentage of individual ^{64}Cu and ^{14}C-sucrose in the CSF outflow. The data in Figure 8C revealed that the percentage of ^{64}Cu radioactivity in the CSF outflow was significantly higher in Mn-treated animals than the controls ($p < 0.05$), so was the ratio of ^{64}Cu/^{14}C-sucrose in the outflow of CSF ($p < 0.05$). Thus, it seemed likely that *in vivo* Mn exposure significantly reduced the efflux of Cu by the BCB.

^{64}Cu retention by choroidal Z310 cells following in vitro *Mn exposure or siRNA knockdown.* To investigate the consequence of altered ATP7A and ATP7B in the BCB, we used Z310 cells to determine the cellular retention of ^{64}Cu following siRNA knockdown of Cu-ATPases and after Mn exposure. The siRNA transfection system was optimized by using qPCR and Western blot to obtain the optimal concentrations of *Atp7a* and *Atp7b* siRNA, which would induce the knockdown but not affected the cell viability. Our data showed that introduction of 80nM *Atp7a* siRNA for 48 h resulted in significant reductions of the

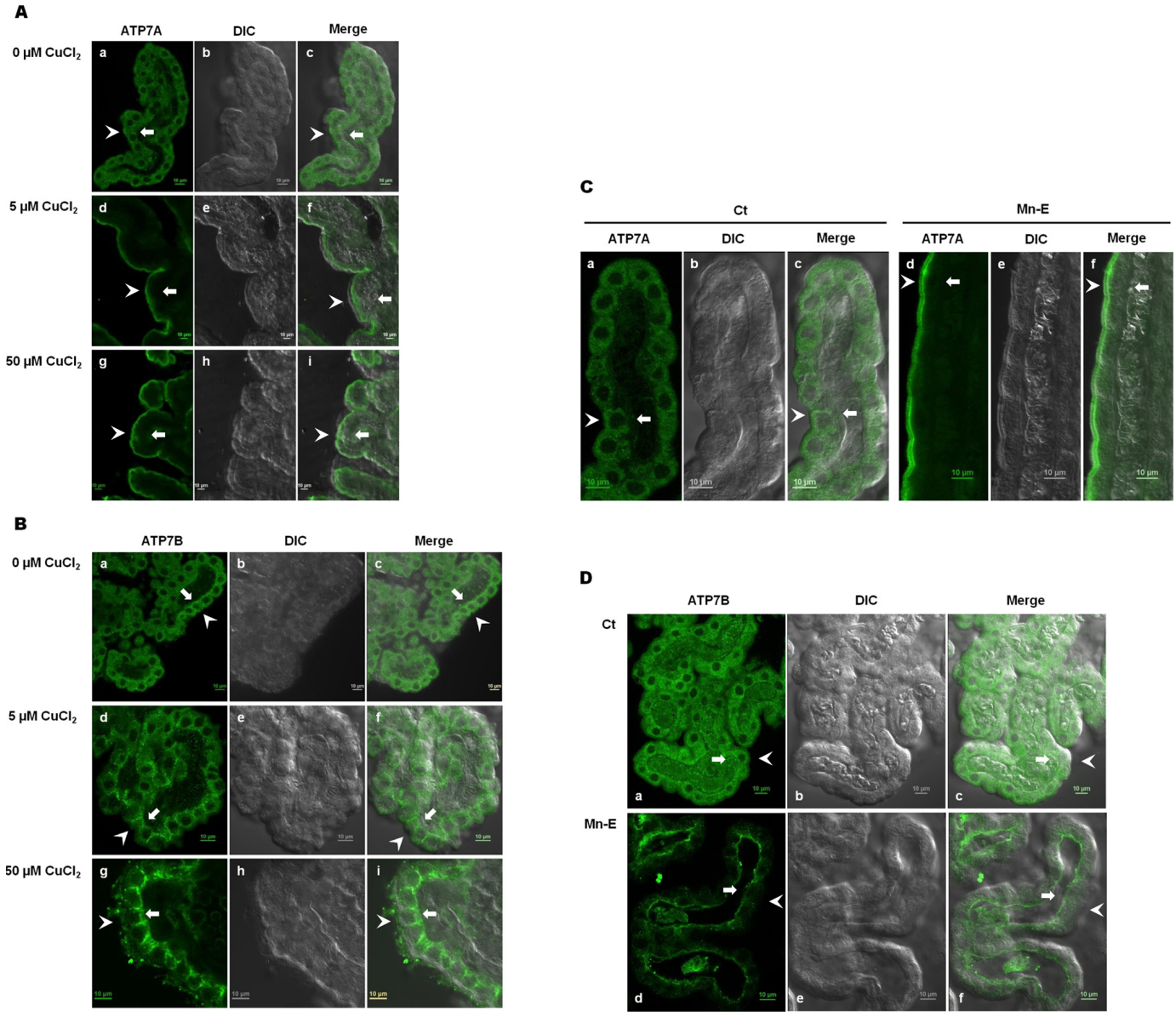

FIG. 6. Subcellular trafficking of ATP7A and ATP7B in the choroid plexus. (A) Subcellular trafficking of ATP7A in freshly isolated choroid plexus tissues following *in vitro* Cu incubation. (a, d, and g) ATP7A fluorescent signals; (b, e, and h) DIC images; (c, f, and i) merged images. (B) Subcellular trafficking of ATP7B in freshly isolated choroid plexus tissues following *in vitro* Cu incubation. (a, d, and g) ATP7B fluorescent signals; (b, e, and h) DIC images; (c, f, and i) merged images. (C) Subcellular trafficking of ATP7A in choroid plexus tissues following *in vivo* subchronic Mn exposure. (a and d) ATP7A fluorescent signals; (b and e) DIC images; (c and f) merged images. (D) Subcellular trafficking of ATP7B in choroid plexus tissues following *in vivo* subchronic Mn exposure. (a and d) ATP7B fluorescent signals; (b and e) DIC images; (c and f) merged images. Arrow head: pointing the apical membrane of choroidal epithelia facing the CSF; arrow: pointing the basolateral membrane of choroidal epithelia facing the blood

mRNA 47 and 41% of the regular control and negative siRNA control, respectively ($p < 0.01$, Supplementary fig. 2A). When transfected Z310 cells with 40nM *Atp7b* siRNA for 48 h, the mRNA level was 28% less than the regular and negative control ($p < 0.01$, Supplementary fig. 2B); the similar knockdown effect was determined when using 80nM *Atp7b* siRNA (Supplementary fig. 2B). Thus, we chose 80nM *Atp7a* siRNA and 40nM *Atp7b* siRNA for Western blot analyses. The results showed that compared with regular and negative siRNA controls, the transfection resulted in a significant knockdown of *Atp7a* (39 and 32% reductions, respectively, $p < 0.01$) and *Atp7b* (35 and 41% reductions, respectively, $p < 0.01$) (Supplementary figs. 2C–F).

Once the condition for siRNA knockdown was established, we performed the ^{64}Cu retention time-course experiments. At the end of transfections and Mn exposure, Z310 cells were incubated with 5 μCi $^{64}CuCl_2$/ml for 1, 2, 4, 8, 12, and 24 h,

TABLE 5
Mn and Cu Concentrations in Serum, CSF, and Choroid Plexus Tissue Following *in vivo* Subchronic Mn Exposure

Group	Serum (μg/l)		CSF (μg/l)		CP (μg/g tissue)	
	Mn	Cu	Mn	Cu	Mn	Cu
Ct	6.15 ± 1.92	1031.5 ± 110.5	4.50 ± 2.08	26.25 ± 4.38	0.27 ± 0.07	1.41 ± 0.16
Mn-E	50.8 ± 30.8**	1437.5 ± 382.8*	51.8 ± 10.9**	52.5 ± 25.9*	2.23 ± 0.15**	2.91 ± 0.38**

Note. Data represent mean ± SD, $n = 4$–8. CSF, CP, Ct, and Mn-E represent cerebrospinal fluid, choroid plexus, control, and Mn-exposed groups, respectively.
*$p < 0.05$, as compared with the control.
**$p < 0.01$, as compared with the control.

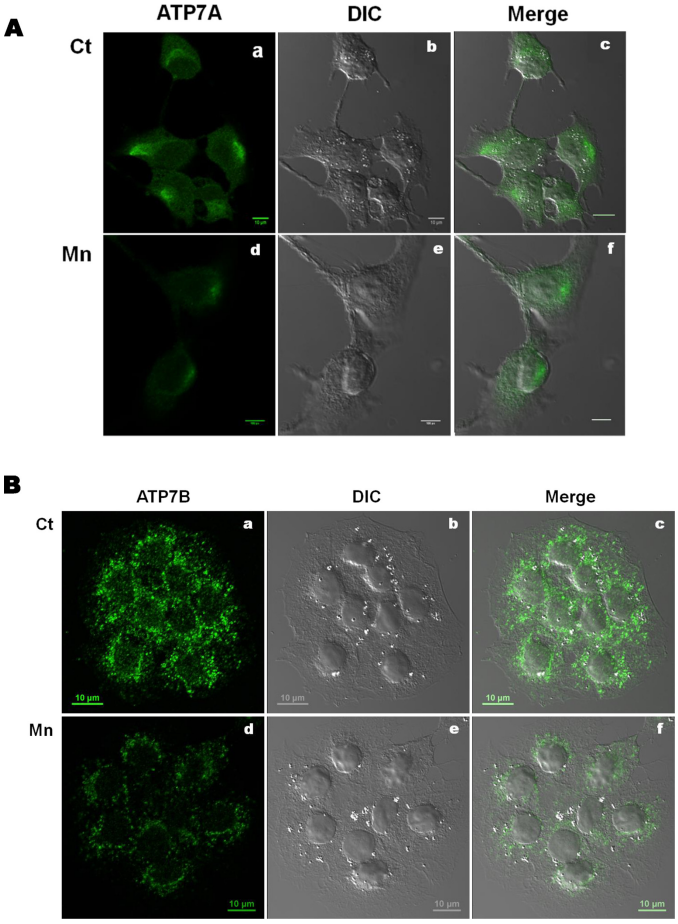

FIG. 7. Subcellular distributions of ATP7A and ATP7B in choroidal epithelial Z310 cells following *in vitro* Mn exposure. (A) ATP7A studies. (a and d) ATP7A fluorescent signals; (b and e) DIC images; and (c and f) merged images. (B) ATP7B studies. (a and d) ATP7B fluorescent signals; (b and e) DIC images; (c and f) merged images. Ct: control group, Mn: Mn-exposed group.

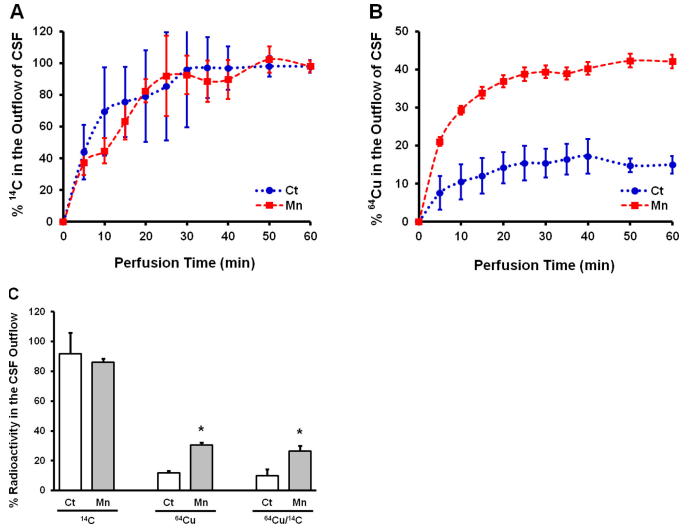

FIG. 8. Decreased Cu clearance by the BCB following *in vivo* subchronic Mn exposure. (A) % ^{14}C radioactivity in the CSF outflow. (B) % ^{64}Cu radioactivity in the CSF outflow. (C) The data of last five time points of the outflow radioactivity during steady-state were used to quantify the steady state of ^{14}C, ^{64}Cu, and ^{64}Cu/^{14}C in the outflow of CSF. Data represent means ± SD, $n = 3$; *$p < 0.05$, when compared with the control.

and followed by three washes with PBS to remove the extracellular isotope for further counting. Data in Table 6 showed that the ^{64}Cu radioactivity in Mn-exposed Z310 cells with 1 h ^{64}Cu incubation was 1.9-fold higher than that in control cells ($p < 0.01$). No significant cellular ^{64}Cu retention was observed in *Atp7a*-knockdown Z310 cells, whereas significant higher cellular ^{64}Cu levels were detected in *Atp7b*-knockdown cells in all time points except the 2 h incubation than those in negative siRNA treated-cells ($p < 0.05$, Table 6). In the presences of both Mn and *Atp7b* siRNA, more ^{64}Cu retained inside the cells than those cells of regular control ($p < 0.01$) and negative siRNA control ($p < 0.05$) following 2, 4, 8, 12, and 24 h incubations (Table 6). Thus, Mn-induced reduction of ATP7B weakened cells' capability to expel intracellular Cu ions.

Reduced ^{64}Cu efflux from the CSF to blood following in vitro *Mn exposure or siRNA knockdown.* As the BCB regulates the material fluxes between the blood and CSF, it was logical to question whether Mn effects on ATP7A and ATP7B expressions ultimately affected Cu transport across the BCB. Thus, we used a well-developed *in vitro* Transwell transport model to study Cu transport by the BCB. The primary choroid plexus epithelial cells were cultured in the inner chamber, which was inserted in the outer chamber. The formation of an impermeable

TABLE 6
Intracellular ^{64}Cu Retention (DPM/μg Protein) in Z310 Cells Following Mn Exposure or siRNA Knockdown

Group	Time point (h)					
	1	2	4	8	12	24
Ct	2.42 ± 0.28	5.16 ± 1.06	12.6 ± 3.46	21.8 ± 2.02	37.9 ± 3.97	425 ± 84.2
NCt	4.35 ± 1.20	6.15 ± 1.59	15.5 ± 5.23	20.1 ± 4.24	38.1 ± 5.41	292 ± 28.8
Mn-E	4.54 ± 1.09**	3.93 ± 0.74	17.2 ± 2.48	23.9 ± 2.39	37.0 ± 4.79	371 ± 147
Atp7a siRNA	3.99 ± 1.18	4.52 ± 1.18	20.9 ± 8.00	23.3 ± 2.46	40.3 ± 4.36	267 ± 71.2
Atp7b siRNA	5.49 ± 0.87$^{\#,\diamond\diamond}$	7.84 ± 2.18$^{\Delta\Delta,\diamond\diamond}$	29.8 ± 7.00$^{\#\#,\Delta\Delta,\diamond\diamond}$	80.7 ± 5.26$^{\#\#,\Delta\Delta,\diamond\diamond}$	217 ± 40.3$^{\#\#,\Delta\Delta,\diamond\diamond}$	1139 ± 144$^{\#\#,\Delta\Delta,\diamond\diamond}$
Mn + *Atp7a* siRNA	2.75 ± 0.79$^{\#\#,\Delta,\diamond}$	7.51 ± 2.35$^{*,\Delta\Delta,\diamond\diamond}$	15.0 ± 2.73	19.4 ± 1.35$^{\Delta,\diamond}$	34.0 ± 1.83	237 ± 50.6
Mn + *Atp7b* siRNA	4.14 ± 0.54§	8.04 ± 1.53$^{**,\#,\Delta\Delta}$	35.9 ± 3.33$^{**,\#\#,\Delta\Delta}$	87.1 ± 3.39$^{**,\#\#,\Delta\Delta,\S\S}$	200 ± 17.3$^{**,\#\#,\Delta\Delta}$	2503 ± 1175$^{**,\#\#,\Delta\Delta,\S\S}$

Note. Data represent mean ± SD, $n = 4$–9. Ct, NCt, and Mn-E represent control, negative siRNA control, and Mn-exposed groups, respectively.
$^{*}p < 0.05$, as compared with the control.
$^{**}p < 0.01$, as compared with the control.
$^{\#}p < 0.05$, as compared with the negative siRNA control.
$^{\#\#}p < 0.01$, as compared with the negative siRNA control.
$^{\Delta}p < 0.05$, as compared with the Mn-E group.
$^{\Delta\Delta}p < 0.01$, as compared with the Mn-E group.
$^{\diamond}p < 0.05$, as compared with the *Atp7a* siRNA group.
$^{\diamond\diamond}p < 0.01$, as compared with the *Atp7a* siRNA group.
$^{\S}p < 0.05$, as compared with the *Atp7b* siRNA group.
$^{\S\S}p < 0.01$, as compared with the *Atp7b* siRNA group.

barrier between the two chambers was judged by three criteria: (1) the cell culture reached the monolayer confluence; (2) the culture medium in the inner chamber was constantly about 2–3 mm higher than the level of medium in the outer chamber; and (3) the TEER value across the cell monolayer was about 50–65 Ω cm^2. About 12 days in the culture, the cells formed the barrier that met the aforementioned criteria (Supplementary fig. 3A). Measurement of radioactivity from the receiver chamber over the time course allowed for estimation of the permeability constant (P_E). Table 7 summarizes the efflux P_E values for ^{64}Cu and ^{14}C-sucrose.

Our early studies using the same *in vitro* Transwell model have established that the efflux of Cu across the BCB is a more favorable pathway for Cu transport than the influx (Monnot *et al.*, 2011). Thus, this study was focused exclusively on the effect of Mn on the Cu efflux. By correcting ^{64}Cu permeability with the space marker ^{14}C-sucrose, it was apparent that the extent of Cu efflux was significantly decreased by 11.7% ($p < 0.01$) and 10.3% ($p < 0.05$), as compared with the regular control or the control with negative siRNA, respectively (Table 7). Similar to the outcomes by Mn exposure, siRNA knockdown of *Atp7a* and *Atp7b* significantly reduced the Cu efflux. Moreover, *Atp7a* and *Atp7b* knockdown along with Mn exposure decreased the Cu efflux P_E value by 12.2 and 15.4%, respectively, as compared with the regular control ($p < 0.01$). Significant decreases of P_E values and P_E ratios were also observed when the siRNA-treated groups were compared with the negative siRNA control ($p < 0.05$). These data suggest that Mn exposure reduced Cu efflux transport by the BCB. Noticeably also, the TEER values in all the treatment groups were significantly decreased (Supplementary fig. 3B); however, the P_E data on ^{14}C-sucrose in Table 7 suggested that there was no significant leakage of the barrier. These observations support a role of ATP7A and ATP7B in Cu transport by the BCB.

DISCUSSION

Our previous studies have suggested that free Cu ions are the major Cu specie transported into the brain via BBB, whereas BCB may serve as a regulatory site for Cu in the CSF (Choi and Zheng, 2009; Monnot *et al.*, 2011; Zheng and Monnot, 2012). A recent human study also supports the choroid plexus as a major regulatory site of Cu transport in developing brains (Donsante *et al.*, 2010). Our current *in vivo* perfusion data provide additional evidence to support this view. In control rats, the volumes of distribution (V_d) of ^{64}Cu to brain parenchyma (0.20–0.34 ml/g) were higher than those to brain capillaries in respective regions (0.07–0.20 ml/g), suggesting that Cu ions were readily transported into brain, but not accumulated in cerebral capillaries. In contrast, the V_d of ^{64}Cu in the choroid plexus was 223-fold higher than that in the CSF. Taking into account a steep Cu concentration gradient between serum and CSF (1032 μg/l vs. 26 μg/l), it is reasonable to conclude that the BCB in the plexus effectively restricts the passage of Cu from blood to CSF. Hence, the transport of Cu into brain parenchyma apparently takes place at the BBB rather than the BCB. Moreover, our *in situ* VC perfusion data revealed that a significant portion of infused ^{64}Cu in the lateral ventricle was transported out of the brain by the plexus, which is in agreement with our previous Transwell data that the direction of BCB in transporting Cu is from the CSF to blood (Monnot *et al.*, 2011). Taken together, these data suggest that the BBB appears to play a role in transporting Cu ions from the blood to brain parenchyma, whereas the BCB plays a role in removing Cu from the CSF to blood.

What function do ATP7A and ATP7B play in transporting Cu at brain barriers? A faster turnover of ATP7A than ATP7B has been reported by Kühlbrandt (2004). By comparing mRNA expression levels of ATP7A and ATP7B in the same BBB or BCB samples, we found that ATP7A was about 13-fold higher than ATP7B in BBB, whereas ATP7B was about sixfold higher than ATP7A in BCB. Thus, at the BBB, ATP7A appears to play

TABLE 7
Efflux Permeability Constants (P_E) of ^{64}Cu and ^{14}C-Sucrose Following Mn Exposure or siRNA Knockdown

Group	P_E value		P_E ratio
	^{14}C	^{64}Cu	$^{64}Cu/^{14}C$
Ct	11.82 ± 0.36	23.55 ± 0.59	1.99 ± 0.10
NCt	11.91 ± 0.30	23.19 ± 1.97	1.94 ± 0.17
Mn-E	11.77 ± 0.24	20.80 ± 1.49$^{**,\#}$	1.77 ± 0.12$^{*,\#}$
Atp7a siRNA	11.79 ± 0.32	20.82 ± 1.96$^{**,\#}$	1.77 ± 0.18$^{*,\#}$
Atp7b siRNA	11.83 ± 0.23	20.92 ± 2.10$^{*,\#}$	1.77 ± 0.16$^{*,\#}$
Mn + *Atp7a* siRNA	11.87 ± 0.10	20.67 ± 2.00$^{**,\#}$	1.74 ± 0.17$^{**,\#}$
Mn + *Atp7b* siRNA	11.60 ± 0.33	19.93 ± 1.37$^{**,\#\#}$	1.72 ± 0.13$^{**,\#}$

Note. Data represent mean ± SD, $n = 5$–6. Ct, NCt, and Mn-E represent control, negative siRNA control, and Mn-exposed groups, respectively
$^{*}p < 0.05$, as compared with the control.
$^{**}p < 0.01$, as compared with the control.
$^{\#}p < 0.05$, as compared with the negative siRNA control.
$^{\#\#}p < 0.01$, as compared with the negative siRNA control.

a predominant role in chauffeuring Cu from the blood to brain. Noticeably, there is a discrepancy between our current and previous report (Choi and Zheng, 2009); the precious study by qPCR had suggested a higher ATP7A mRNA expression in the BCB. This discrepancy is due to the reference tissue used in the calculation. The previous study used the brain parenchyma as the reference (100%) to normalize expression values of ATP7A and ATP7B in brain capillaries and choroid plexus. The current method by comparing the relative difference of ATP7A and ATP7B in the same tissues and cell lines is deemed to be more accurate in reflecting the relative abundance of two Cu transporters in brain barriers.

Unlike in the BBB, both ATP7A and ATP7B appear to play roles in transporting Cu ions across the BCB. Our confocal data clearly showed that Cu treatment alone led to the movement of intracellular ATP7A from the perinuclear location to the apical microvilli of choroidal epithelia, and that ATP7B moved in the opposite direction toward the basal membrane facing the blood. Our observations thus confirm the hypothesis proposed by Kaler (2011) that in the BCB the trafficking of ATP7A is presumably oriented toward the apical microvilli, whereas ATP7B may move to the basolateral membrane so to transport Cu from the CSF to blood. Donsante *et al.* (2011) have also confirmed that choroid plexus is a useful therapeutic target for regulating Cu homeostasis in the CNS due to the rich expression of ATP7A in choroidal epithelia, suggesting that the choroid plexus mediates the delivery of Cu ions into the brain. Considering the recently discovered para-vascular pathway (Iliff *et al.*, 2012), we would caution that the efflux of Cu by the choroid plexus may not be the sole pathway for Cu to leave the CSF.

Compelling evidences have demonstrated that Mn ions are capable of crossing both BBB and BCB and accumulating in brain tissues and choroid plexus without causing direct injury to barrier structures (Aschner and Gannon, 1994; Michotte *et al.*, 1977; Valois and Webster, 1989; Zheng *et al.*, 1998). Our AAS results consistently showed that Mn was highly concentrated in selected brain regions and choroid plexus following *in vivo* Mn exposure (Zheng *et al.*, 2009). In agreement with previous animal and human studies (Guilarte *et al.*, 2006; Jiang *et al.*, 2007; Lai *et al.*, 1999; Wang *et al.*, 2008a; Zheng *et al.*, 2009), we also observed a significant elevation of Cu concentrations in striatum, choroid plexus, CSF and serum of Mn-exposed animals. However, no significant changes were observed in the Cu levels of hippocampus and frontal cortex. A high accumulation of Mn in globus pallidus and nearby striatal area is one of the clinical features by MRI in manganese patients (Dydak *et al.*, 2011; Jiang *et al.*, 2007). Thus, it seems likely that the higher Mn accumulation may lead to a more selectively effect on Cu regulatory mechanism in striatal area than in other brain areas. It is also possible that the Cu regulatory mechanism may be different from one brain area to another owing to the structural and functional differences of brain regional barriers (Zheng, 2001a,b).

Three possible mechanisms may explain Mn-induced Cu dyshomeostasis: (1) Mn may increase the transport of Cu from blood into parenchyma via BBB; (2) Mn may decrease the clearance of Cu from CSF by acting on the BCB, rendering Cu being retained in CSF; and (3) Mn may replace Cu in its storage and consequently increase Cu in brain extracellular fluids. Because Mn exposure significantly reduced expressions of both ATP7A and ATP7B in the BBB, it seemed unlikely that there would be sufficient ATP7A to increase Cu influx into brain parenchyma via the BBB route. Our *in situ* VC perfusion and *in vitro* Transwell studies, on the other hand, suggested a significant reduction of Cu efflux in the BCB following Mn exposure. Thus, we postulate that a hindered Cu efflux in the BCB, which is mediated by ATP7B that is diminished following Mn exposure, may be responsible for increased Cu concentrations in the CSF as well as in selected brain regions.

Aside from ATP7A and ATP7B, Mn exposure has been shown to affect other metal transport proteins, i.e., divalent metal transporter-1 (DMT1), Cu transport protein (CTR1), and ferroportin (Fpn)) (Madejczyk and Ballatori, 2012; Monnot

et al., 2012; Wang *et al.*, 2006; Yin *et al.*, 2010; Zheng *et al.*, 2012; Zheng and Monnot, 2012). Whether Mn exposure affects DMT1 and CTR1 in the BBB is unknown; however, increased expressions of DMT1 and CTR1 in the BCB have been established in Mn-exposed animals (Wang *et al.*, 2006; Zheng and Monnot, 2012). Our recent studies using Z310 cell-based tetracycline (Tet)-inducible CTR1 or DMT1 expression cell lines suggest that Tet-induced CTR1 elevation can lead to a robust increase of ^{64}Cu uptake, whereas the induction of DMT1 by Tet results in only a slight increase of ^{64}Cu uptake regardless the substantial increase in DMT1 protein expression (Zheng *et al.*, 2012). Thus, we conclude that CTR1, but not DMT1, plays an essential role in transporting Cu by the BCB. It should be noticed also that *in vivo* Mn exposure can lead to the translocation of CTR1 from the cytosol to the apical microvilli of choroidal epithelia, where the protein apparently fails to return to the cytosol (Zheng and Monnot, 2012). Thus, the combination of the dysfunctional CTR1 and diminished efflux mechanism mediated by ATP7B upon Mn exposure may explain the increased Cu level in brain extracellular fluids.

This study has several limitations. First, Mn exposure has been associated with a decreased mRNA expression of metallothionein (MT), a major cytoplasmic protein for Cu storage, in cultured rat astrocytes and the developing rat brain (Erikson and Aschner, 2002; Weber *et al.*, 2002). As a result of reduced MT, more Cu ions may be released into the cytoplasm or cerebral interstitial fluid. The current study as designed is unable to test this hypothesis. Second, although Mn exposure has been found to interrupt the cellular ATP production, how exactly this impairment affects Cu-ATPases regarding their expression and intracellular trafficking remains unknown. Third, due to the technical limitation in studying the directional transport of materials in BBB, the current study is unable to confirm the subcellular trafficking of ATP7A and ATP7B in brain capillary endothelia.

In summary, this study establishes that Cu is transported by BBB from blood to brain parenchyma, which is likely mediated by ATP7A in brain capillary cells. By the concentration gradient, Cu ions move from interstitial space between neurons and glial cells into the CSF, where CTR1 in the apical surface of BCB takes Cu into choroidal epithelial cells. Within the BCB, ATP7B transports Cu ions to the basolateral membrane and expels them into the blood circulation. Mn exposure inhibits ATP7A and ATP7B expression and function, leading to a hindered efflux of Cu by the BCB. This may contribute to Mn-induced dyshomeostasis of Cu in the CNS.

SUPPLEMENTARY DATA

Supplementary data are available online at http://toxsci.oxfordjournals.org/.

FUNDING

National Institute of Health/National Institute of Environmental Health Sciences (RO1-ES008146).

ACKNOWLEDGMENTS

The RBE4 cell line was a kind gift from Dr Michael Aschner at Vanderbilt University. The polyclonal antirabbit ATP7A antibody used for Z310 cells immunofluorescent staining was provided by Dr James Gitlin at Vanderbilt University.

REFERENCES

Arredondo, M., Munoz, P., Mura, C. V., and Nunez, M. T. (2003). DMT1, a physiologically relevant apical Cu^{1+} transporter of intestinal cells. *Am. J. Physiol. Cell Physiol.* **284**, C1525–C1530.

Aschner, M., and Gannon, M. (1994). Manganese (Mn) transport across the rat blood-brain barrier: Saturable and transferrin-dependent transport mechanisms. *Brain Res. Bull.* **33**, 345–349.

Barbeau, A., Inoué, N., and Cloutier, T. (1976). Role of manganese in dystonia. *Adv. Neurol.* **14**, 339–352.

Bocca, B., Alimonti, A., Senofonte, O., Pino, A., Violante, N., Petrucci, F., Sancesario, G., and Forte, G. (2006). Metal changes in CSF and peripheral compartments of parkinsonian patients. *J. Neurol. Sci.* **248**, 23–30.

Chodobski, A., and Segal, M. B. (2005). In vivo techniques used in blood-CSF barrier research: Measurement of CSF formation. In: *The Blood-Cerebrospinal Fluid Barrier* (W. Zheng and A. Chodobski, Eds.), pp. 595–605. CRC Press, New York.

Choi, B. S., and Zheng, W. (2009). Copper transport to the brain by the blood-brain barrier and blood-CSF barrier. *Brain Res.* **1248**, 14–21.

Crossgrove, J. S., Li, G. J., and Zheng, W. (2005). The choroid plexus removes beta-amyloid from the cerebrospinal fluid. *Exp. Biol. Med.* **230**, 771–776.

Crossgrove, J. S., and Zheng, W. (2004). Manganese toxicity upon overexposure. *NMR Biomed.* **17**, 544–553.

Deane, R., Zheng, W., and Zlokovic, B. V. (2004). Brain capillary endothelium and choroid plexus epithelium regulate transport of transferrin-bound and free iron into the rat brain. *J. Neurochem.* **88**, 813–820.

Donsante, A., Johnson, P., Jansen, L. A., and Kaler, S. G. (2010). Somatic mosaicism in Menkes disease suggests choroid plexus-mediated copper transport to the developing brain. *Am. J. Med. Genet. A* **152A**, 2529–2534.

Donsante, A., Yi, L., Zerfas, P. M., Brinster, L. R., Sullivan, P., Goldstein, D. S., Prohaska, J., Centeno, J. A., Rushing, E., and Kaler, S. G. (2011). ATP7A gene addition to the choroid plexus results in long-term rescue of the lethal copper transport defect in a Menkes disease mouse model. *Mol. Ther.* **19**, 2114–2123.

Dydak, U., Jiang, Y. M., Long, L. L., Zhu, H., Chen, J., Li, W. M., Edden, R. A. E., Hu, S. G., Fu, X., Long, Z. Y., *et al.* (2011). In vivo measurement of brain GABA concentrations by magnetic resonance spectroscopy in smelters occupationally exposed to manganese. *Environ. Health Perspect.* **119**, 219–224.

Erikson, K. M., and Aschner, M. (2002). Manganese causes differential regulation of glutamate transporter (GLAST) taurine transporter and metallothionein in cultured rat astrocytes. *Neurotoxicology* **23**, 595–602.

Gaggelli, E., Kozlowski, H., Valensin, D., and Valensin, G. (2006). Copper homeostasis and neurodegenerative disorders (Alzheimer's, Prion, and Parkinson's diseases and amyotrophic lateral sclerosis). *Chem. Rev.* **106**, 1995–2044.

Gorell, J. M., Johnson, C. C., Rybicki, B. A., Peterson, E. L., Kortsha, G. X., Brown, G. G., and Richardson, R. J. (1999). Occupational exposure to manganese, copper, lead, iron, mercury and zinc and the risk of Parkinson's disease. *Neurotoxicology* **20**, 239–247.

Guilarte, T. R., and Chen, M. K. (2007). Manganese inhibits NMDA receptor channel function: Implications to psychiatric and cognitive effects. *Neurotoxicology* **28**, 1147–1152.

Guilarte, T.R., McGlothan, J.L., Degaonkar, M., Chen, M.K., Barker, P.B., Syversen, T., and Schneider, J.S. (2006) Evidence for cortical dysfunction and widespread manganese accumulation in the nonhuman primate brain following chronic manganese exposure: a 1H-MRS and MRI study.. *Toxicol Sci*, **94**, 351–358.

Hozumi, I., Hasegawa, T., Honda, A., Ozawa, K., Hayashi, Y., Hashimoto, K., Yamada, M., Koumura, A., Sakurai, T., Kimura, A., *et al.* (2011). Patterns of levels of biological metals in CSF differ among neurodegenerative disease. *J. Neurol. Sci.* **303**, 95–99.

Iliff, J. J., Wang, M., Liao, Y., Plogg, B. A., Peng, W., Gundersen, G. A., Benveniste, H., Vates, G. E., Deane, R., Goldman, S. A., *et al.* (2012), A paravascular pathway facilitates CSF flow through the brain parenchyma and the clearance of interstitial solutes, including amyloid b. *Sci. Transl. Med.* **4**, 147ra111.

Iwase, T., Nishimura, M., Sugimura, H., Igarashi, H., Ozawa, F., Shinmura, K., Suzuki, M., Tanaka, M., and Kino, I. (1996). Localization of Menkes gene expression in the mouse brain: Its associateion with neurological manifestation in Menkes model mice. *Acta Neuropathol.* **91**, 482–488.

Jiang, Y. M., Mo, X. A., Du, F. Q., Fu, X., Zhu, X. Y., Gao, H. Y., Xie, J. L., Liao, F. L., Pira, E., and Zheng, W. (2006). Effective treatment of manganese-induced occupational parkinsonism with p-aminosalicylic acid: A case of 17-year follow-up study. *J. Occup. Environ. Med.* **48**, 644–649.

Jiang, Y. M., Zheng, W., Long, L. L., Zhao, W. J., Li, X. R., Mo, X. A., Lu, J. P., Fu, X., Li, W. M., Liu, S. F., *et al.* (2007). Brain magnetic resonance imaging and manganese concentrations in red blood cells of smelting workers: Search for biomarkers of manganese exposure. *Neurotoxicology* **28**, 126–135.

Kaler, S. G. (2011). ATP7A-related copper transport diseases—Emerging concepts and future trends. *Nat. Rev. Neurol.* **7**, 15–29.

Kiaei, M., Bush, A. I., Morrison, B. M., Morrison, J. H., Cherny, R. A., and Volitakis, I. (2004). Genetically decreased spinal cord copper concentration prolongs life in a transgenic mouse model of amyotrophic lateral sclerosis. *J. Neurosci.* **24**, 7945–7950.

Kuo, Y. M., Gitschier, J., and Packman, S. (1997). Developmental expression of the mouse mottled and toxic milk genes suggests distinct functions for the Menkes and Wilson disease copper transporters. *Hum. Mol. Genet.* **6**, 1043–1049.

Kühlbrandt, W. (2004). Biology, structure and mechanism of P-type ATPases. *Nat. Rev. Mol. Cell Biol.* **5**, 282–295.

Lagrange, P., Romero, I. A., Minn, A., and Revest, P. A. (1999). Transendothelial permeability changes induced by free radicals in an in vitro model of the blood-brain barrier. *Free Radic. Biol. Med.* **27**, 667–672.

Lai, J. C., Minski, M. J., Chan, A. W., Leung, T. K., and Lim, L. (1999). Manganese mineral interactions in brain. *Neurotoxicology* **20**, 433–444.

Livak, K. J., and Schmittgen, T. D. (2001). Analysis of relative gene expression data using real-time quantitative PCR and the 2 (-Delta Delta C(T)) method. *Methods* **25**, 402–408.

Li, G. J., Zhao, Q., and Zheng, W. (2005). Alteration at translational but not transcriptional level of transferring receptor expression following manganese exposure at the blood-CSF barrier in vitro. *Toxicol. Appl. Pharmacol.* **205**, 188–200.

Madejczyk, M. S., and Ballatori, N. (2012). The iron transporter ferroportin can also function as a manganese exporter. *Biochim. Biophys. Acta* **1818**, 651–657.

Malhi, H., Irani, A.N., Volenberg, I., Schilsky, M.L., and Gupta, S. (2002) Early cell transplantation in LEC rats modeling Wilson's disease eliminates hepatic copper with reversal of liver disease.. *Gastroenterology*, **122**, 438–447.

Michotte, Y., Massart, D. L., Lowenthal, A., Knaepen, L., Pelsmaekers, J., and Collard, M. (1977). A morphological and chemical study of calcification of the choroid plexus. *J. Neurol.* **216**, 127–133.

Monnot, A. D., Behl, M., Ho, S., and Zheng, W. (2011). Regulation of brain copper homeostasis by the brain barrier systems: Effects of Fe-overload and Fe-deficiency. *Toxicol. Appl. Pharmacol.* **256**, 249–257.

Monnot, A. D., and Zheng, W. (2012). Culture of choroid plexus epithelial cells and in vitro model of blood-CSF barrier. In *Epithelial Cell Culture Protocols, Methods in Molecular Biology*, 2nd ed. (S. R. Randell and M. L. Fulcher Eds.), Vol. **945**, pp. 13–29. Springer Science+Business Media, LLC.

Monnot, A. D., Zheng, G., and Zheng, W. (2012). Mechanism of copper transport at the blood-cerebrospinal fluid barrier: Influence of iron deficiency in an in vitro model. *Exp. Biol. Med. (Maywood)* **237**, 327–333.

Nyasae, L., Bustors, R., Braiterman, L., Eipper, B., and Hubbard, A. (2007) Dynamics of endogenous ATP7A (Menkes protein) in intestinal epithelial cells: copper-dependent redistribution between two intracellular sites.. *Am J Physiol Gastrointest Liver Physiol*, **292**, G1181–G1194.

Parenti, M., Rusconi, L., Gappabianca, V., Parati, E. A., and Groppetti, A. (1988). Role of dopamine in manganese neurotoxicity. *Brain Res.* **473**, 236–240.

Petris, M. J., Mercer, J. F. B., Culvenor, J. G., Lockhart, P., Gleeson, P. A., and Camakaris, J. (1996). Ligand-regulated transport of the Menkes copper P-type ATPase efflux pump from the Golgi apparatus to the plasma membrane: A novel mechanism of regulated trafficking. *EMBO J.* **15**, 6084–6095.

Preston, J. E., al-Sarraf, H., and Segal, M. B. (1995). Permeability of the developing blood-brain barrier to 14C-mannitol using the rat in situ brain perfusion technique. *Brain Res. Dev. Brain Res.* **87**, 69–76.

Qian, Y., Tiffany-Castiglioni, E., Welsh, J., and Harris, E. D. (1998). Copper efflux from murine microvascular cells requires expression of Menke's disease Cu-ATPase. *J. Nutr.* **128**, 1276–1282.

Racette, B. A., Aschner, M., Guilarte, T. R., Dydak, U., Criswell, S. R., and Zheng, W. (2012). Pathophysiology of manganese-associated neurotoxicity. *Neurotoxicology* **33**, 881–886.

Reaney, S. H., and Smith, D. R. (2005). Manganese oxidation state mediates toxicity in PC 12 cells. *Toxicol. Appl. Pharmacol.* **205**, 271–281.

Régina, A., Romero, I., Greenwood, J., Adamson, P., Bourre, J., Couraud, P., and Roux, F. (1999). Dexamethasone regulation of P-glycoprotein activity in an immortalized rat brain endothelial cell line GPNT. *J. Neurochem.* **73**, 1954–1963.

Shi, L. Z., and Zheng, W. (2005). Establishment of an in vitro brain barrier epithelial transport system for pharmacological and toxicological study. *Brain Res.* **1057**, 37–48.

Sparks, L. S., and Schreurs, B. G. (2003). Trace amounts of copper in water induce b-amyloid plagues and learning deficits in a rabbit model of Alzheimer's disease. *Proc. Natl. Acad. Sci. U.S.A.* **100**, 11065–11069.

Squitti, R., Bressi, F., Pasqualetti, P., Bonomini, C., Ghidoni, R., Binetti, G., Cassetta, E., Moffa, F., Ventriglia, M., Vernieri, F., *et al.* (2009). Longitudinal prognostic value of serum "free" copper in patients with Alzheimer disease. *Neurology* **72**, 50–55.

Strausak, D., Mercer, J. F., Dieter, H. H., Stremmel, W., and Multhaup, G. (2001). Copper in disorders with neurological symptoms: Alzheimer's, Menkes, and Wilson diseases. *Brain Res. Bull.* **55**, 175–185.

Strozyk, D., Launer, L. J., Adlard, P. A., Cherny, R. A., Tsatsanis, A., Volitakis, I., Blennow, K., Petrovitch, H., White, L. R., and Bush, A. I. (2009). Zinc and copper modulate Alzheimer Aβ levels in human cerebrospinal fluid. *Neurobiol. Aging* **30**, 1069–1077.

Uchino, A., Noguchi, T., Nomiyama, K., Takase, Y., Nakazono, T., Nojiri, J., and Kudo, S. (2007) Manganese accumulation in the brain: MR imaging.. *Neuroradiology*, **49**, 715–720.

Valois, A. A., and Webster, W. S. (1989). Retention and distribution of manganese in the mouse brain following acute exposure on postnatal day 0, 7, 14 or 42: An autoradiographic and gamma counting study. *Toxicology* **57**, 315–328.

Vescovi, A., Facheris, L., Zaffaroni, A., Malanca, G., and Parati, E. A. (1991). Dopamine metabolism alterations in a manganese-treated pheochromocytoma cell line (PC12). *Toxicology* **67**, 129–142.

Wang, D. X., Du, X. Q., and Zheng, W. (2008a). Alteration of saliva and serum concentrations of manganese, copper, zinc, cadmium and lead among career welders. *Toxicol. Lett.* **176**, 40–47.

Wang, X. Q., Li, G. J., and Zheng, W. (2006). Upregulation of DMT1 expression in choroidal epithelial of the blood-CSF barrier following manganese exposure in vitro. *Brain Res.* **1097**, 1–10.

Wang, X. Q., Li, G. J., and Zheng, W. (2008b). Efflux of iron from the cerebrospinal fluid to the blood at the blood-CSF barrier: Effect of manganese exposure. *Exp. Biol. Med.* **233**, 1561–1571.

Weber, S., Dorman, D. C., Lash, L. H., Erikson, K., Vrana, K. E., and Aschner, M. (2002). Effects of manganese (Mn) on the developing rat brain: Oxidative-stress related endpoints. *Neurotoxicology* **23**, 169–175.

Yang, J., and Aschner, M. (2003). Developmental aspects of blood–brain barrier (BBB) and rat brain endothelial (RBE4) cells as in vitro model for studies on chlorpyrifostransport. *Neurotoxicology* **24**, 741–745.

Yin, Z., Jiang, H., Lee, E. Y., Ni, M., Erikson, K. M., Milatovic, D., Bowman, A. B., and Aschner, M. (2010). Ferroportin is a manganese-responsive protein that decreases manganese cytotoxicity and accumulation. *J. Neurochem.* **112**, 1190–1198.

Zheng, W. (2001a). Toxicology of choroid plexus: Special reference to metal-induced neurotoxicities. *Microsc. Res. Tech.* **52**, 89–103.

Zheng, W. (2001b). Neurotoxicology of the brain barrier system: New implications. *J. Toxicol. – Clin. Toxicol.* **39**, 711–719.

Zheng, G., Chen, J., and Zheng, W. (2012). Relative contribution of CTR1 and DMT1 in copper transport by the blood-CSF barrier: Implication in manganese-induced neurotoxicity. *Toxicol. Appl. Pharmacol.* **260**, 285–293.

Zheng, W., Jiang, Y. M., Zhang, Y. S., Jiang, W., Wang, X. Q., and Cowan, D. M. (2009). Chelation therapy of manganese intoxication by para-aminosalicylic acid (PAS) in Sprague-Dawley rats. *Neurotoxicology* **30**, 240–248.

Zheng, W., Kim, H., and Zhao, Q. (2000). Comparative toxicokinetics of manganese chloride and methylcyclopentadienyl manganese tricarbonyl (MMT) in Sprague-Dawley rats. *Toxicol. Sci.* **54**, 295–301.

Zheng, W., and Monnot, A. D. (2012). Regulation of brain iron and copper homeostasis by brain barrier systems: Implication in neurodegenerative diseases. *Pharmacol. Ther.* **133**, 177–188.

Zheng, W., Ren, S., and Graziano, J. H. (1998). Manganese inhibits mitochondrial aconitase: A mechanism of manganese neurotoxicity. *Brain Res.* **799**, 334–342.

Zheng, W., and Segal, M. B. (2005). In situ techniques used in the blood-CSF barrier research. In: *The Blood-Cerebrospinal Barrier* (W. Zheng and A. Chodobski, Eds.), pp. 541–551. CRC Press, New York.

Zheng, W., and Zhao, Q. (2002). Establishment and characterization of an immortalized Z310 choroidal epithelial cell line from murine choroid plexus. *Brain Res.* **958**, 271–380.

Zheng, W., Zhao, Q., Slavkovich, V., Aschner, M., and Graziano, J. H. (1999). Alteration of iron homeostasis following chronic exposure to manganese in rats. *Brain Res.* **833**, 125–132.

Zhou, B., and Gitschier, J. (1997). hCTR1: A human gene for copper uptake identified by complementation in yeast. *Proc. Natl. Acad. Sci. U.S.A.* **94**, 7481–7486.